T-1081

SOLID STATE PHASE RELATIONSHIPS IN THE SODIUM-POTASSIUM-ANTIMONY TERNARY SYSTEM

By

Carlos A. Villachica

T-1081

A thesis respectfully submitted to the Faculty and the Board of Trustees of the Colorado School of Mines in partial fulfillment of the requirements for the degree of Master of Science in Metallurgical Engineering.

Signed: Carlos A. Villachica
Carlos A. Villachica

Golden, Colorado
Date: May 12, 1966

Approved: Paul G. Herold
Paul G. Herold
Thesis Advisor

A. W. Schlechten
A. W. Schlechten
Head of Department

Golden, Colorado
Date: May 12, 1966

ABSTRACT

The solid state phase relationships of the ternary sodium-potassium-antimony system have been studied by standard X-ray diffraction procedures, using powder samples enclosed in pyrex capillary tubes. The initial mixtures were prepared in a specially conditioned "dry box" under dry nitrogen atmosphere. All compositions were heat treated in a Lindberg tube furnace under a protective atmosphere of purified argon gas.

A set of binary alloys was prepared to check the phase relationships established by previous investigators on the two binary alloy series, Na-Sb and K-Sb. The Na-Sb alloy series was found to be well established, and the present study agrees with the work done by Mathewson(1); but in the K-Sb alloy series two more compounds were found which had been overlooked by Parravano (2). The results indicated that these two compounds have the formulas KSb_2 and K_5Sb_4.

Based on the binary compounds involved in this study, a series of ternary alloys was prepared to determine the Alkemade triangles. When this study was begun, the author did not have knowledge of the existence of the compound Na_2KSb previously discovered by Sommer (3) to aid in

determining the Alkemade lines. A new ternary compound having a composition corresponding to the formula K_2NaSb was found. Unlimited solid solubility was discovered in the field between K_2NaSb and K_3Sb in the pseudo-binary section drawn through Na_3Sb, Na_2KSb, K_2NaSb and K_3Sb. Consequently, this gave two two-phase regions inside of the diagram, bounded by the triangles K_5Sb_4-K_3Sb-NaK_2Sb and K_3Sb-NaK_2Sb-K, respectively. Since no other visible solid solubilities were found, they may be considered negligibly small. The isothermal section of this ternary phase diagram at room temperature showed the presence of twelve Alkemade triangles.

The melting temperatures of the new phases found in this study were determined by thermal analysis techniques. Na_2KSb melts congruently at 667°C; NaK_2Sb melts congruently at 618°C; K_5Sb_4 melts incongruently at 509°C; and KSb_2 melts congruently at 409°C.

TABLE OF CONTENTS

LIST OF ILLUSTRATIONS

LIST OF TABLES

LIST OF APPENDICES

ACKNOWLEDGMENTS

The author wishes to express his particular indebtedness to Dr. Paul G. Herold, Research Professor of Ceramic and Metallurgical Engineering, for his continuous interest and guidance throughout this study.

The author also wishes to express his appreciation to the Colorado School of Mines Foundation, Incorporated, for providing a research assistanceship in connection with this investigation.

Grateful acknowledgment is extended to Cerro de Pasco Corporation for granting the author a one-year scholarship, followed by a continued leave of absence in order that this study could be completed.

INTRODUCTION

The properties of intermetallic compounds formed by alkali metals and elements of the V-A group of the periodic system, have been studied for various reasons. Zintl and co-workers (4) investigated these compounds to clarify their crystal chemistry, and in particular to determine the boundary at which the transition of the type of bonding of alloys from metallic to ionic takes place.

In 1936 Gorlich (5) discovered the excellent photoemissivity of Cs_3Sb. Since then, many semi-conducting photoemissive materials have been found. These materials have the characteristic of being intermetallic compounds of alkali metals with metals of the IVth, Vth, or VIth group of the periodic system. In all compounds containing a single alkali metal, the threshold wavelength increases with the atomic number of the alkali metal involved, so that the cesium compound is always the most sensitive to visible radiation.

The Sb-Cs cathode is outstanding among these materials because it has high photosensitivity, is simple to produce, and has been the subject of numerous experimental studies aimed at a better understanding of the photoelectric mechanism.

The excellent performance of the Sb-Cs photocathode indicated that the material should have a well-defined chemical composition. Quantitative studies by Sommer (6) suggested the stoichiometric formula Cs_3Sb. Jack and Wachtel (7) determined the crystal structure of Cs_3Sb and found it had a partially ordered structure based upon the B32 sodium thallide type. They also attempted to correlate the photoelectric properties of the compound with the crystal structure.

Although cesium is superior to other alkali metals in all types of cathodes, Sommer (3) found that the combination of two or more alkali metals with antimony leads, in some cases, to photocathodes with a sensitivity higher -- especially at long wavelengths -- than that of Cs_3Sb. This "multi-alkali effect" has been definitely established for two cathodes of the general formulae Sb-K-Na and Sb-K-Na-Cs. In the formation process for these cathodes, the introduction of the alkali metals needs to be carefully controlled because it appears that the ratio in the final layer is critical. The Sb-K-Na-Cs cathode covers the visible spectrum more effectively than any other known photoemitter. These combinations of antimony with alkali metals have the stoichiometric formula SbM_3. Chemical analysis indicated that the optimum ratio of sodium to potassium was approximately 2 to 1, both in the Sb-K-Na and the Sb-K-Na-Cs cathodes. The amount of cesium in the latter is of a very small order.

Although Sommer (3) presented some data which help explain the "multi-alkali effect," the metal compounds formed in the photocathode

are unknown at present. Because of this lack of information, it is very difficult to prepare films which consistently possess high sensitivity. In order to clarify the difficulties, it is necessary to establish the sodium-potassium-antimony three-component diagram. Cesium is ignored since Spicer (8) points out that the cesium acts only to increase the electron affinity. Therefore, the three components apparently combine to form the light converter, whereas cesium merely amplifies the effect (9).

The phase equilibria of the elements used to form the photoemissive surfaces are not known for other than the two component systems. Previous investigations had determined the phase relationships between Na-Sb, K-Sb, and Na-K; however, knowledge was needed concerning the interaction between the three end members. Aside from the structure determination work on Na_2KSb by Scheer and Zalm (10) and McCarroll (11), little work had been done to determine the interior of the three-phase diagram.

The investigation described in this paper was begun in the belief that knowledge of the three-phase diagram was necessary to work intelligently with any combination between the three end members.

LITERATURE SURVEY

The edges of the three-phase diagram have been completely determined, and are taken from the review by Hansen (12).

Binary Sodium-Potassium System

The binary Na-K phase diagram has been discussed by Hansen (12) and is shown in Fig. 1. This phase diagram indicates an incongruently melting compound, Na_2K, which changes into sodium and liquid at 6.6°C. The eutectic composition is 66.6 at. % K at a temperature of -12.5°C. The compound Na_2K is hexagonal with a structure of the $MgZn_2$ type. The unit cell dimensions are a_0 = 7.5 A.U. and c_0 = 12.30 A.U.

Binary Sodium-Antimony System

Mathewson (1) has studied the alloys of antimony and sodium using thermal and microscopic analysis techniques. Hansen (12) also presented a summary of the work done on this alloy series.

The Na-Sb phase diagram (Fig. 2) shows the existence of two congruent compounds, Na_3Sb and NaSb. The existence of these two intermediate phases were established by Mathewson (1). These intermetallic

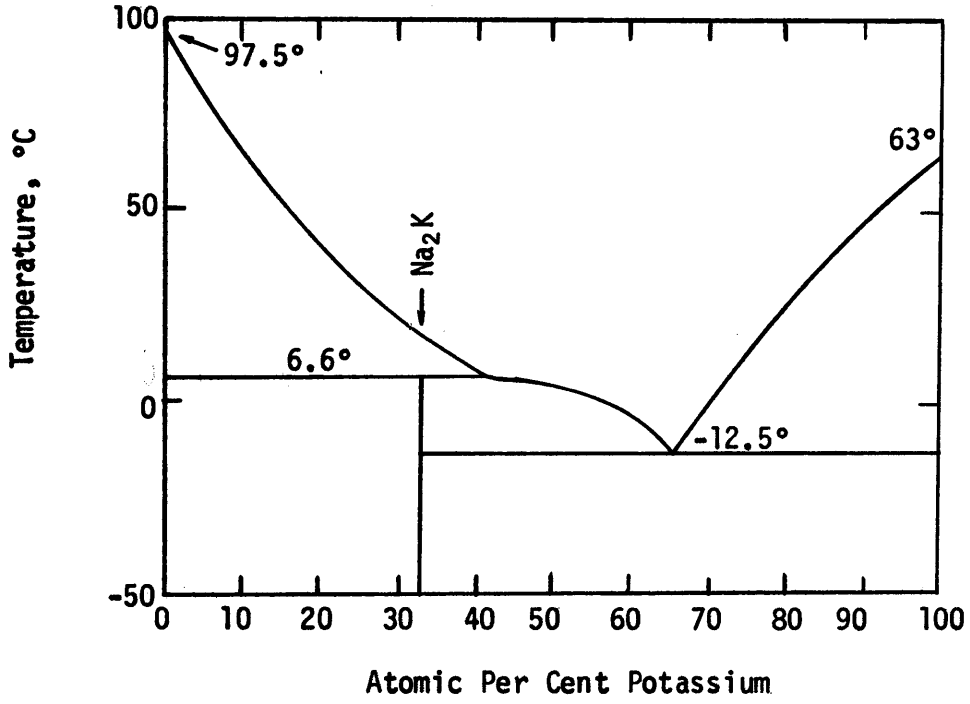

Fig. 1. Potassium-Sodium Equilibrium Diagram (after Hansen (12)).

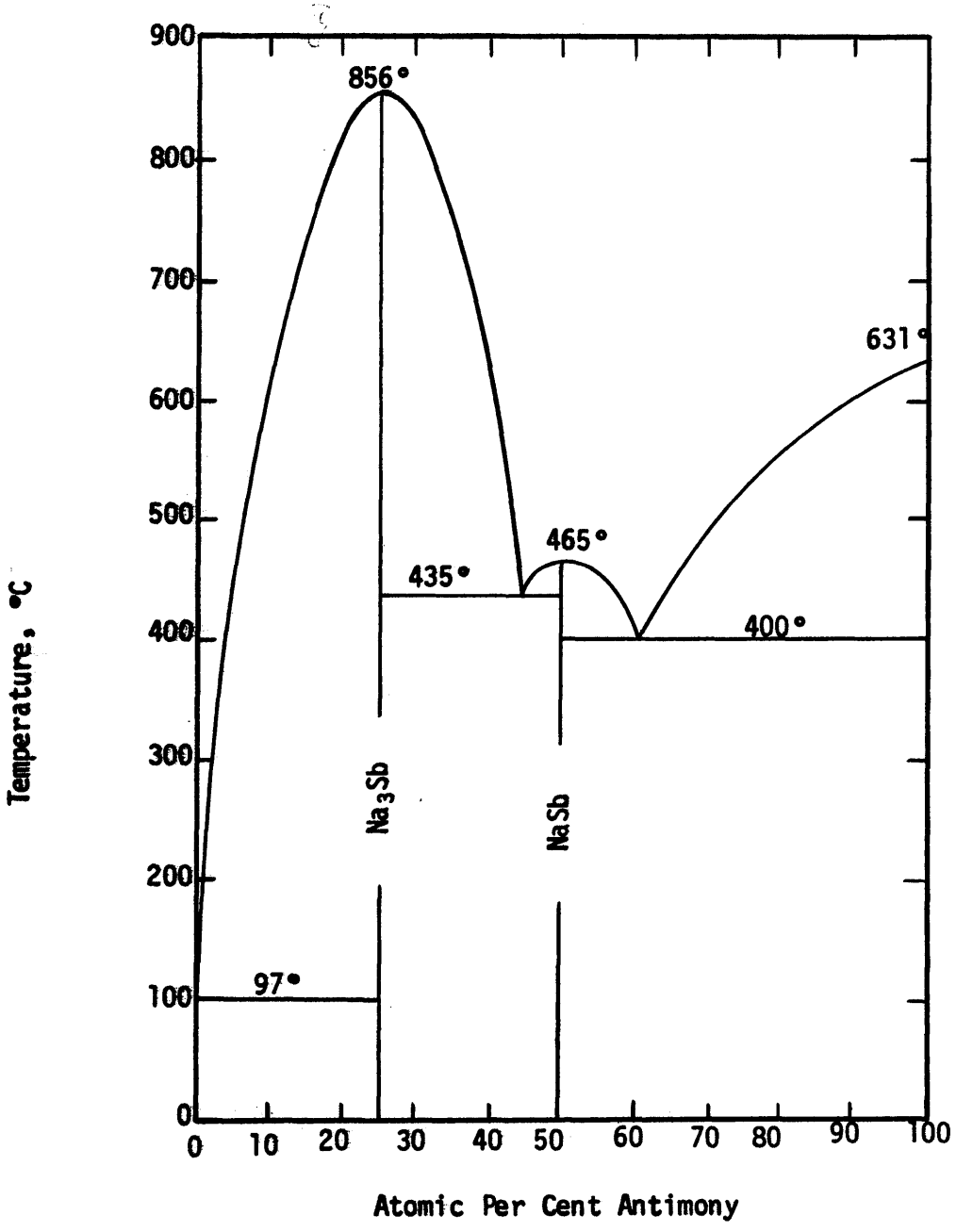

Fig. 2. Sodium-Antimony Equilibrium Diagram (after Mathewson (1)).

compounds divide the diagram into three simple eutectic partial diagrams, representing the Na-Na_3Sb series, the$_3$ Na_3Sb-NaSb series, and the NaSb-Sb series. In the Na-Na_3Sb series, the eutectic solidifies at 97°C and is practically pure sodium. In the Na_3Sb-NaSb series, the eutectic solidifies at 435°C, at 44.5 at. % Sb. In the NaSb-Sb series, the eutectic solidifies at 400°C, at 60.6 at. % Sb. No visible solid solutions were observed.

The compound Na_3Sb melts at 856°C and has the hexagonal Na_3As type of structure, with a unit cell size of a_0 = 5.366 A.U. and c_0 = 9.515 A.U. The compound NaSb melts at 465°C. Zintl and Dullenkopf (4) have described the compound NaSb, reporting it to be monoclinic. However, they did not give the cell dimensions. Cromer (13) has determined the crystal structure of NaSb by single crystal methods and found it to be isostructural with LiAs. The dimensions of the monoclinic cell are a_0 = 6.80 A.U., b_0 = 6.34 A.U., c_0 = 12.48 A.U., and β = 117.6°.

Binary Potassium-Antimony System

The equilibrium diagram of the system K-Sb as given by Hansen (12) is shown in Fig. 3, based on the work of Parravano (2), who used thermal analysis and microscopic techniques.

In essence, the K-Sb system is similar to the binary Na-Sb. It shows two congruent compounds, K_3Sb and KSb. K_3Sb melts at 812°C and has the hexagonal Na_3As type of structure, with a unit cell dimension of a_0 = 6.037 A.U. and c_0 = 10.717 A.U. The KSb melts at 605°C, and its structure has not been determined. Reference to Fig. 3 shows the eutectic

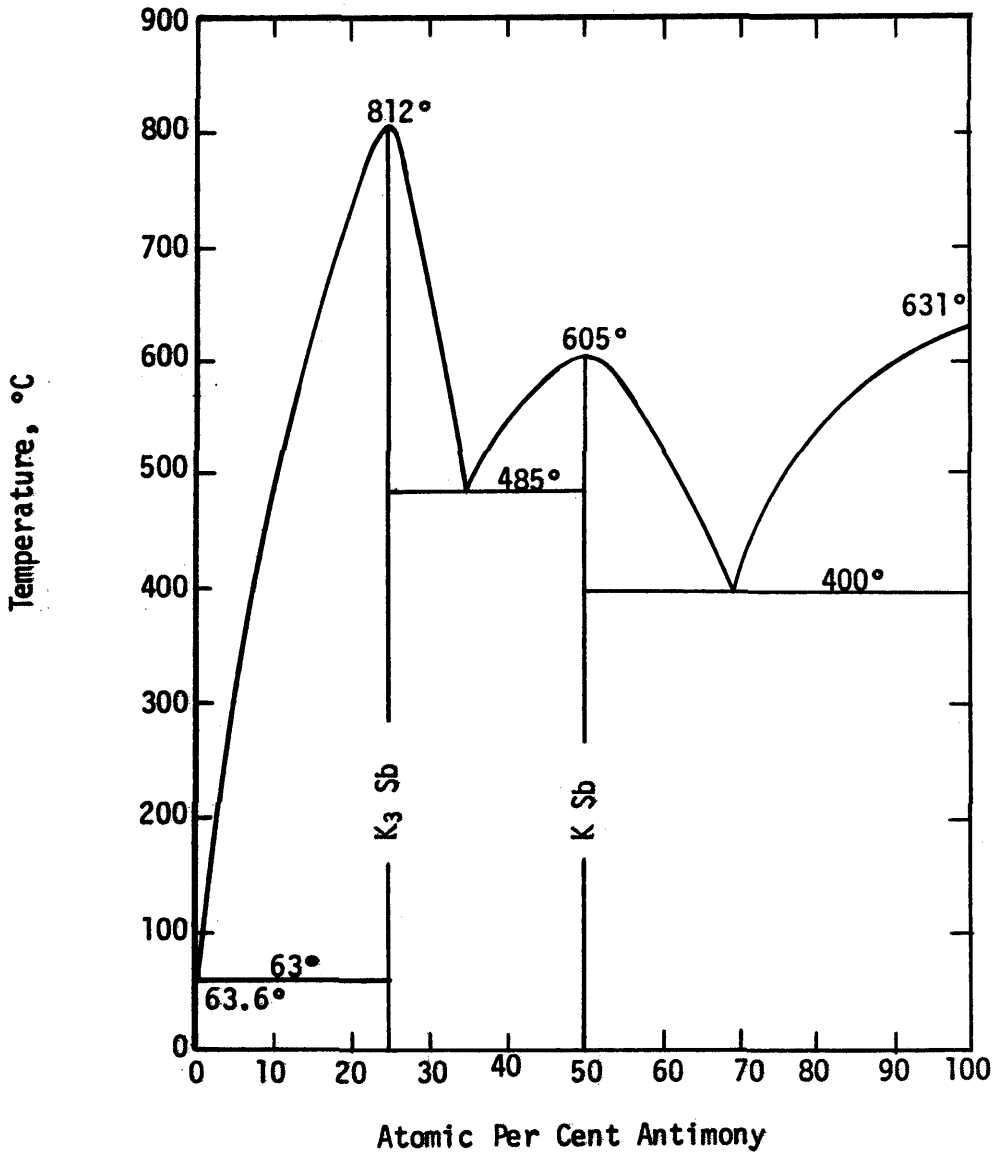

Fig. 3. Potassium-Antimony Equilibrium Diagram (after Parravano (2)).

K + K_3Sb solidifying at 63°C to be practically pure potassium; the eutectic K_3Sb + KSb solidifying at 485°C, at 61.2 at. % Sb; and the eutectic KSb + Sb solidifying at 400°C, at 24.2 at. % Sb. Solid solubilities were not observed.

Ternary Sodium-Potassium-Antimony System

For photoemissive work, and in the knowledge that combinations of alkali metals with antimony in the 3 to 1 ratio had good photoemissive properties, Sommer (3) suggested the compound Na_2KSb. Scheer and Zalm (10) first, and McCarroll (11) later, determined its crystal structure. Both results agreed fully and showed the compound Na_2KSb to be face-centered-cubic with a unit cell dimension of a_0 = 7.724 A.U., and having the same structure as the ferromagnetic Heusler alloy, Cu_2MnAl. Aside from these investigations, no definite study on any particular section of the ternary Na-K-Sb system had been made until the present investigation.

EXPERIMENTAL APPARATUS AND PROCEDURE

In this investigation, 28 binary and 61 ternary alloys were prepared. Starting with high purity metals (see Appendix I for composition), the alloys were prepared under a protective atmosphere of purified argon gas in a Lindberg tube furnace. X-ray powder samples enclosed in capillary tubes were prepared from the resulting alloys in a specially conditioned "dry box." The results were utilized in drawing the isothermal section of the ternary Na-K-Sb system. Also, the melting temperatures of the newly discovered phases were determined in a specially arranged furnace.

Experimental Apparatus

The apparatus used in this study consisted of five separate units:

(1) a "dry box"

(2) a gas purification train

(3) an alloy heat-treatment furnace unit

(4) a melting temperature determination system

(5) an X-ray diffraction unit.

Dry Box. The dry box (Fig. 4) was used for manipulation of the starting materials and the resulting alloys under a protective atmosphere of dry high purity nitrogen gas.

After extensive repairing and reconditioning of this surplus box, it was flushed out and then filled with high purity dry nitrogen. For weighing purposes a balance was placed inside of it. The dry box proved to be airtight; chips of sodium and potassium metal were used to minimize the oxygen partial pressure within. Humidity was reduced by the use of phosphorus pentoxide (phosphoric acid, anhydride) placed inside.

As shown in Fig. 4, the dry box had two auxiliary chambers, one located on each side of the main box. Both were connected to the main box by airtight doors. The chamber to the left was used to store the metals and alloy specimens; the metallic sodium and potassium were always kept under paraffin oil, and the alloy specimens were kept in closed sample bottles to protect them from oxidation and decomposition within the chamber itself. The chamber to the right was used as a transfer handling chamber opening to the outside atmosphere. The right chamber was equipped with two airtight doors, one facing the main dry box and the other facing the normal atmosphere. At any time, only one door could be open without disturbing the protective and dry atmosphere in the box. When the transferring of an object from normal atmosphere air into the dry box was required, the object was placed inside the handling chamber. The normal atmosphere door was next closed, and the

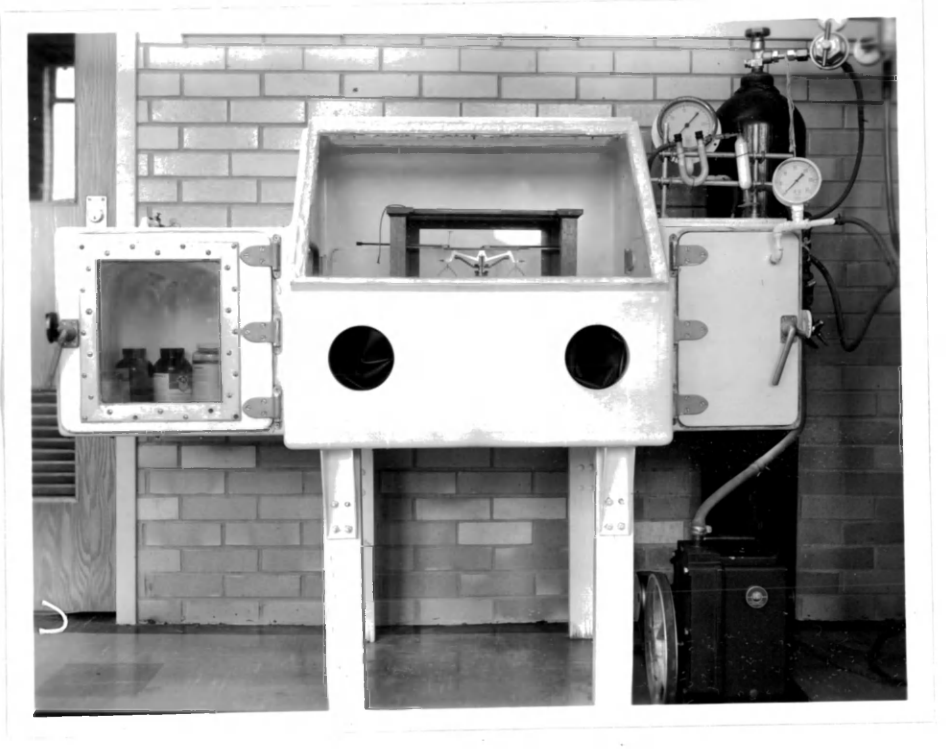

Fig. 4. Photograph of Dry Box

chamber was evacuated by means of a rotary oil pump and then filled with dry nitrogen. This cycle was repeated twice to insure maximum oxygen elimination from the handling chamber. The next step was to again fill the right chamber with dry nitrogen in order to equalize the internal pressure to that of the outside atmosphere. Thereafter the door that gave access to the main dry box could be opened.

Sodium and potassium are very reactive metals; the great affinity of these metals for oxygen enables the formation of oxide coatings even at minute oxygen concentrations. Moisture accelerates this reaction. The oxygen pressures for sodium and potassium metals in equilibrium with their oxides are less than 10^{-100} atmospheres (14), at room temperature. Therefore, to reproduce such a condition is difficult, even more so considering the size of the dry box. The main purpose of this dry box was to slow down the oxidation during manipulation of the initial materials and the resulting alloys. It is of interest to note that, although sodium and potassium metals react with oxygen, freshly cleaned surfaces of these metals remained bright and shiny in the dry nitrogen atmosphere for short periods, giving enough time to allow manipulations such as weighing, grinding, etc.

Gas Purification Train. The purity of the gas used was critical. Although the argon gas available was of high purity, as evidenced by the specifications of the manufacturer (Appendix I), it did contain enough oxygen to cause oxidation, so that purification was necessary.

The oxygen partial pressure in the argon gas was reduced by allowing the gas to flow through a tube filled with copper chips externally heated to 700°C. Oxygen was further reduced by permitting the gas to continue its flow through another tube filled with titanium chips externally heated to 900°C. The partial pressure of oxygen in thermodynamic equilibrium for this purification is given in Appendix II.

Moisture in the gas was reduced to a minimum by passing the gas through a U tube filled with magnesium perchlorate. A greater improvement in drying was further provided by using Drierite and phosphorus pentoxide in separate tubes, in series, at the end of the gas purification step.

No oxidation was encountered in using argon gas in these experiments. The gas purification steps, as established, were considered satisfactory, as indicated by the bright and clean surfaces of the alloys after the heat treatment.

The gas purification train is shown in Figs. 5 and 6. Tank argon was first led through magnesium perchlorate, and secondly through the tubes containing copper and titanium chips. Finally the gas was flowed through the Drierite and phosphorous pentoxide tubes. The gases were then passed through either of the two furnaces employed in this investigation. The exit gases were bubbled through an oil trap to prevent back pressures of air from filtering into the furnaces. The bubbling of argon in this manner also served as an effective monitor to assure that no leaks had developed during a run.

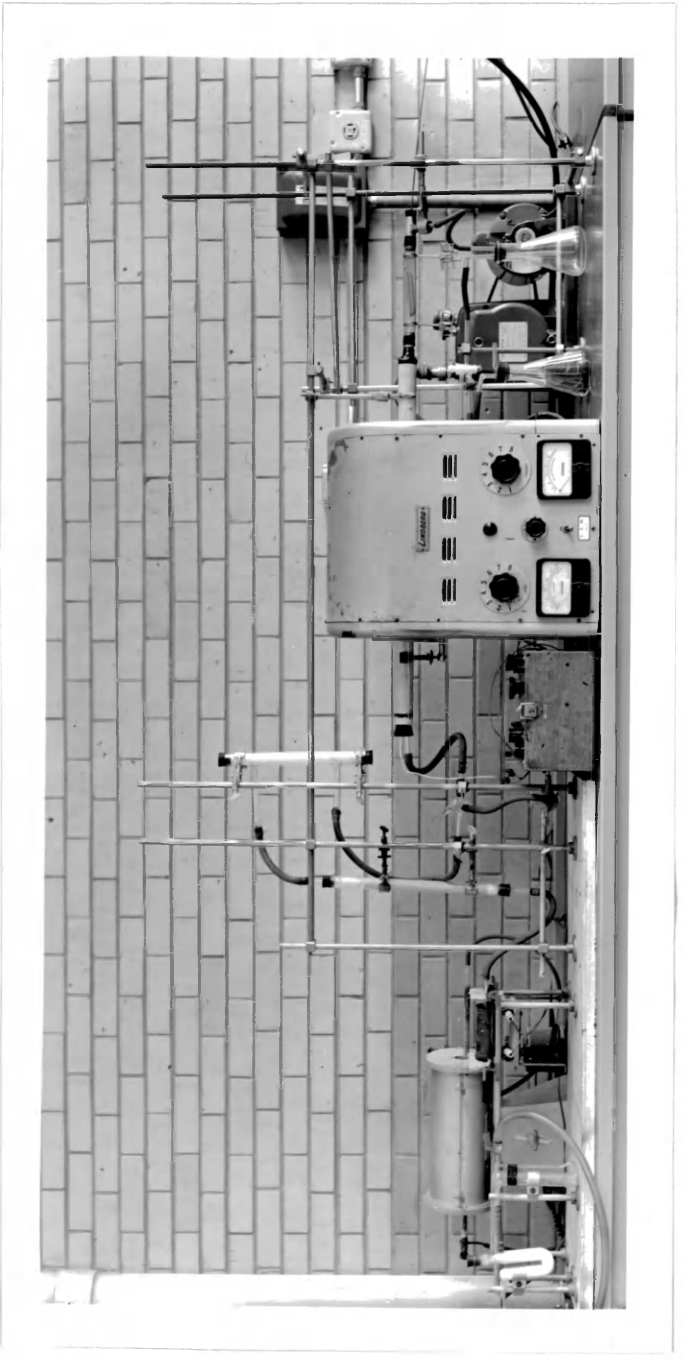

Fig. 5. Photograph of Gas Purification Train and Heat Treatment Furnace

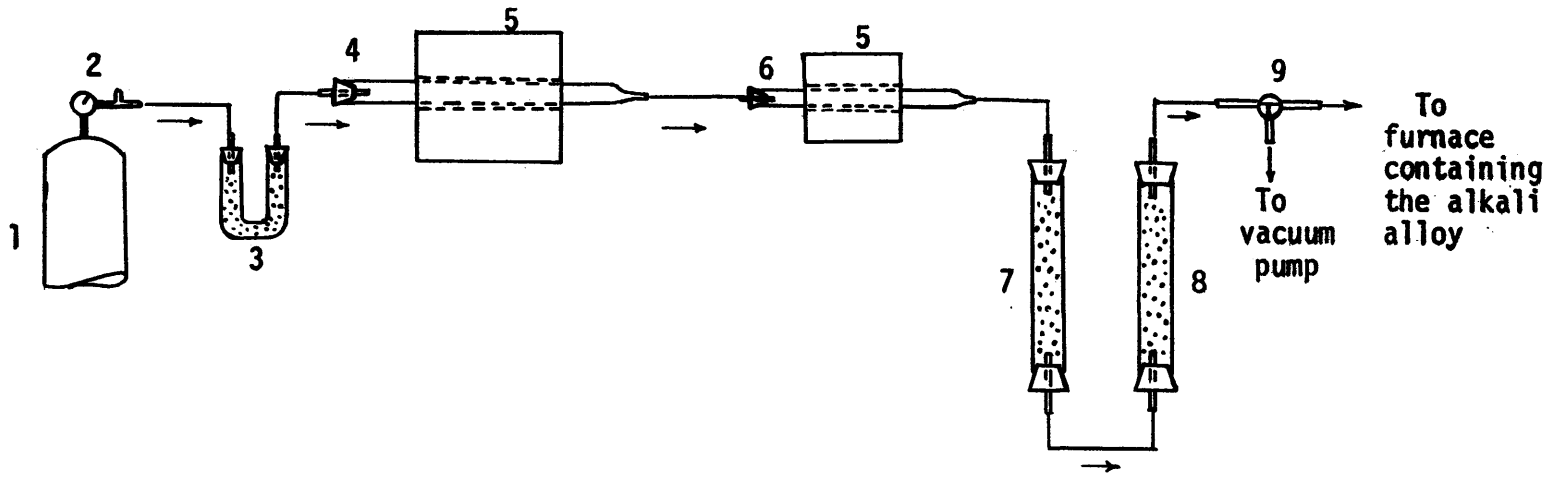

1. Argon gas tank
2. Gas regulator and flow-meter
3. Pyrex U tube containing magnesium perchlorate
4. Vycor tube containing copper turnings
5. Nichrome wound furnaces
6. Vycor tube containing titanium chips
7. Pyrex tube containing drierite
8. Pyrex tube containing magnesium perchlorate
9. Three-way stopcock

Fig. 6. Diagram of the Argon Purification Train.

Alloy Heat-Treatment Furnace Unit. A Lindberg tube furnace with an inner mullite reaction tube 1¼ in. in diameter and 30 in. in length was employed for the preparation of the alloys. Temperature control was provided by a Leeds and Northrup millivolt potentiometer and a 2-foot-long chromel-alumel thermocouple.

The alloys were prepared under an inert atmosphere of purified argon gas. This method was selected in order to avoid any non-desirable impurity pickup by the alloys from the protective gas. Argon gas flowed continuously over the alloys as long as they remained in the furnace unit. The gas flow was regulated at 1 cu ft of argon per hour. Initially, some oxidation was experienced in utilizing the argon gas, but those difficulties were later overcome by careful purification of the gas, as mentioned previously.

The mullite reaction tube was provided with a copper tube insert, 7/8 in. in diameter and 5 in. in length, of which 4 in. extended outside one end of the mullite tube. This copper tube provided an adequate outside diameter, allowing the 7/8-in.-diameter Tygon tubing containing the nickel boat to be joined to the furnace unit. Once this Tygon tubing was set in the proper position, as shown in Figs. 5 and 7, it provided a closed and airtight system. Also, a steel rod that could slide inside the tube furnace was provided. This rod was used to move the nickel boat inside the furnace tube, as necessary. It slid through a rubber stopper opening and still kept the system airtight.

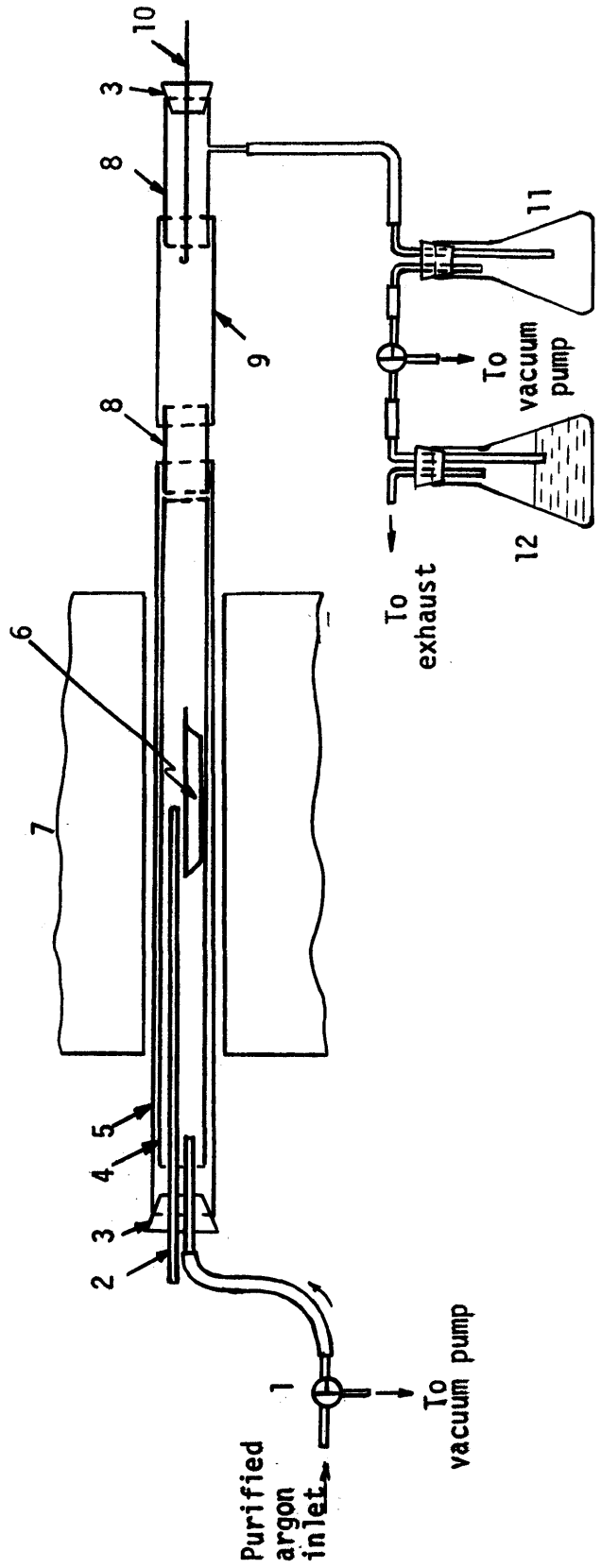

1. Three-way stopcock
2. Thermocouple with Vycor sheath
3. Rubber stopper
4. Steel lining
5. Mullite tube
6. Nickel boat
7. Lindberg furnace
8. Copper tube
9. Tygon tubing
10. Steel rod
11. Erlenmeyer flask trap
12. Oil bubbler

Fig. 7. Diagram of Heat Treatment Furnace Unit.

Melting Temperature Determination System. The apparatus used in the melting temperature determinations of the newly discovered phases consisted of a lagged Nichrome-wound crucible furnace that had a heating chamber 8 in. high and 3 in. in diameter (Figs. 8 and 9). The bottom of the furnace was lagged with asbestos, forming a 2 in. deep base. The electric current through the furnace was reduced, during the determination of a cooling curve, by incorporating a variable voltage transformer. The sliding contact on the transformer was operated by a reduction-geared motor.

Each alloy was placed in a 30 ml Vycor crucible. The crucible was then inserted into a one-end closed mullite tube 14 in. in length and 2 in. in diameter. The upper end of the tube was sealed by a rubber stopper through which two Vycor tubes were passed to permit circulation of a slow current of purified argon gas.

A chromel-alumel thermocouple was used for temperature control. The thermocouple was protected by a stainless-steel sheath, with the individual thermocouple wires separated from each other by MgO powder. A cold reference junction was provided. The two wires of the thermocouple were soldered to copper wires, and the soldered junctions were placed in glass tubes in a constant temperature bath of ice and water contained in a vacuum flask. The copper leads were connected to a Leeds and Northrup potentiometer.

X-ray Diffraction Unit. Powder diffraction photographs of the samples were made at room temperature using a 10-cm Debye-Sherrer camera with a fine focus nickel-filtered copper radiation in a Norelco X-ray unit.

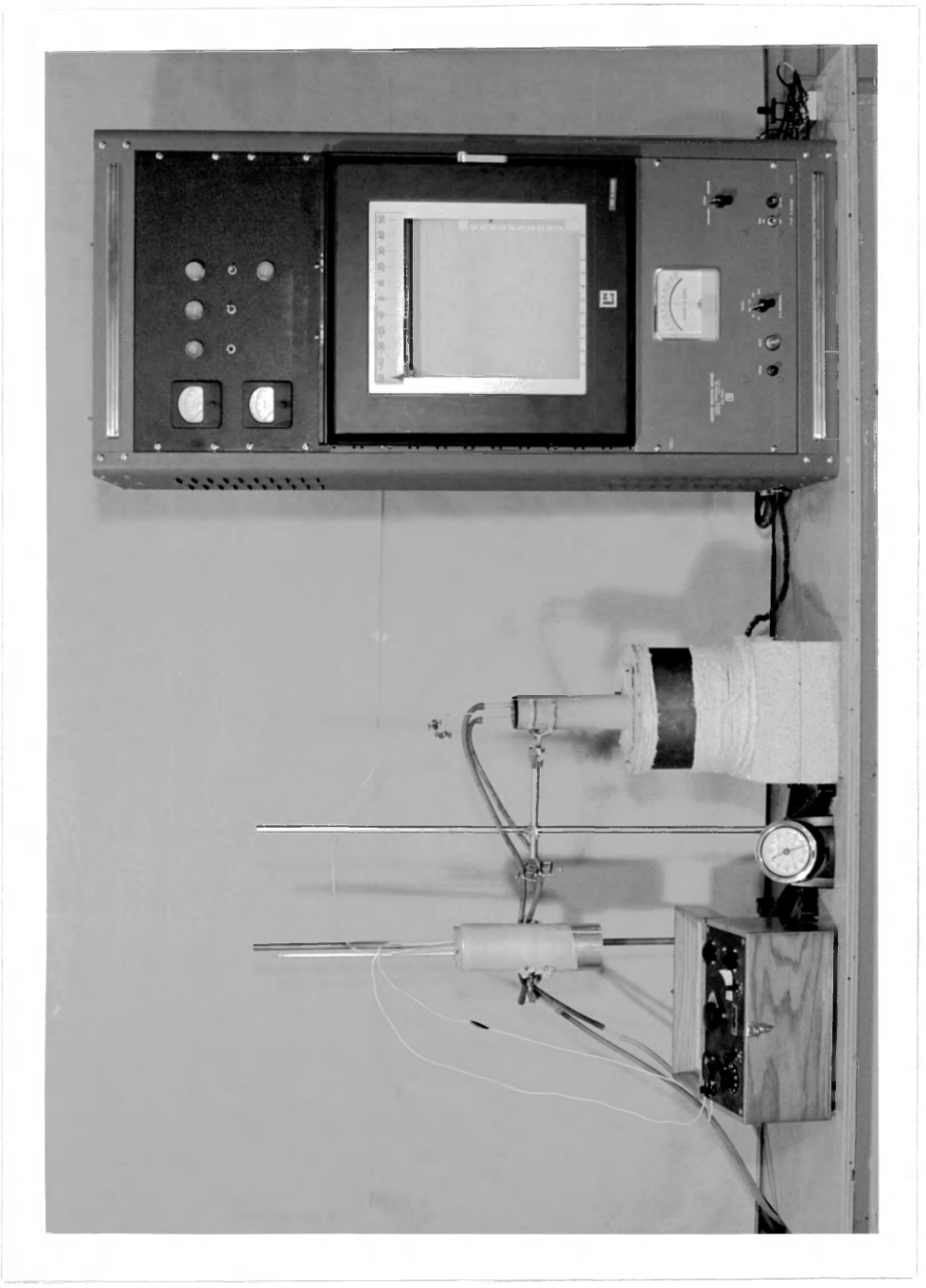

Fig. 8. Photograph of Melting Temperature Determination System

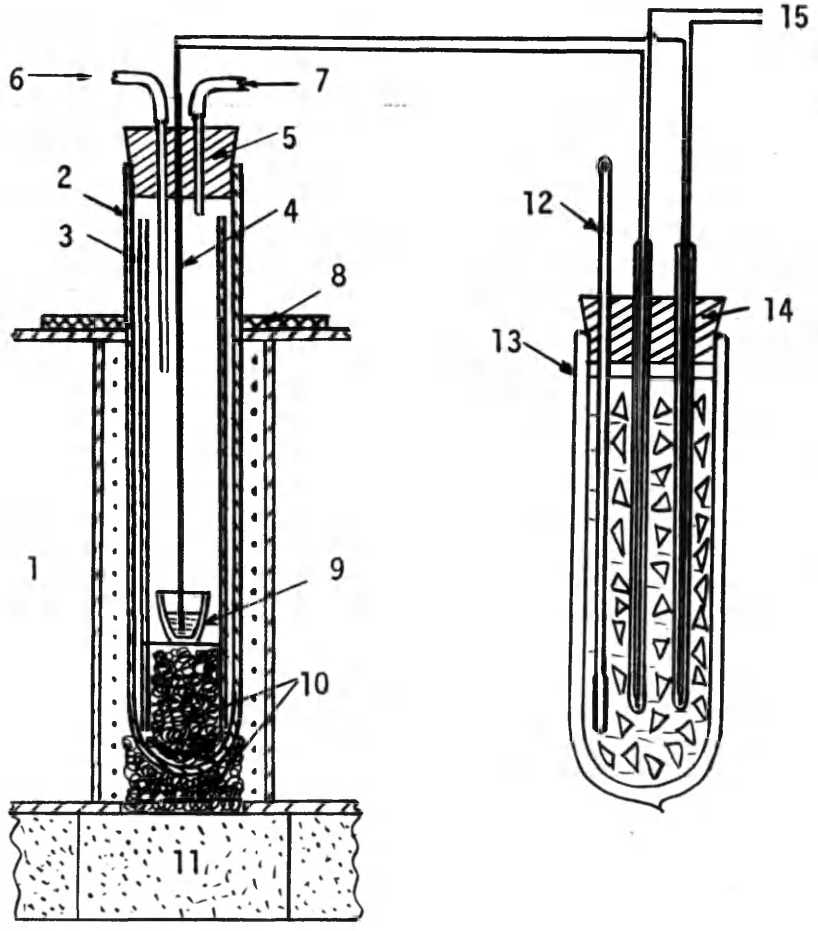

1. Nichrome resistance furnace
2. Outer mullite tube closed at one end
3. Inner mullite tube
4. Chromel-alumel thermocouple with stainless steel sheath wires. Wires separated by MgO powder
5. Rubber stopper
6. Argon inlet
7. Argon outlet
8. Asbestos plate
9. Vycor crucible
10. Asbestos lagging
11. Insulating brick
12. Mercury thermometer
13. Vacuum flask with ice and water
14. Cork stopper
15. Copper leads to potentiometer

Fig. 9. Diagram of Apparatus for Melting Temperature Determination and Ice-Water Cold Junction for Thermocouple.

Experimental Procedure

Since sodium and potassium alloys react readily with oxygen or moisture, it was necessary to perform all handling operations in an extremely dry and oxygen-free medium. For purposes of discussion, the experimental procedure can be conveniently divided into three areas: preparation of the alloys for phase relationship determination, preparation of alloy specimens for X-ray analysis, and melting temperature determination of the new phases found in this study.

Preparation of the Alloys for Phase Relationship Determination. The alloy compositions were prepared by weighing the corresponding amounts of each metal in the dry box. The average weight of the alloy specimens was 15 grams. The weighing was accurate to ±1.0 milligram.

The weighed metals were placed in a 5-in. nickel boat, which in turn was placed inside a piece of Tygon tubing 7/8 in. in diameter and 8 in. in length. This tubing was then clamped on both ends to keep the metals under a protective inert atmosphere while the nickel boat was removed from the dry box and transferred to the furnace.

The tubing containing the nickel boat was placed as indicated in Figs. 5 and 7. Electrician's plastic tape was used to join this tubing to the furnace setup. Apiezon wax was used to prevent leaks. Operating two three-way stopcocks, located one on each side of the tubing containing the nickel boat (Figs. 5 and 7), the system was evacuated by means of a rotary oil pump. Then, manipulating the same stopcocks, the system was isolated from the vacuum pump, and purified argon gas was allowed to flow and fill the setup until inside pressure equaled the atmospheric. At this

stage the clamps from the Tygon tubing were released to allow the argon gas to enter. The gas then passed through a paraffin-oil bubbler trap to prevent back diffusion of air before the gas was exhausted to the atmosphere. Then, the nickel boat was placed in the proper position inside the furnace by means of a steel rod (Figs. 5 and 7), which could slide through the length of the furnace.

The alloying of antimony with alkali metals is an extremely exothermic reaction. The reactions in this study were explosive and produced spattering of the mixture during the vigorous reaction. At the same time, the temperature of the mass rose above 500°C and resulted in a heterogeneous sintered material which made homogenization difficult. The temperature of the alloy had to be taken above 600°C and held at that temperature long enough to effect homogenization. Simultaneously, due to the high vapor pressure of the alkali metals, the weight losses were high enough to make the results uncertain.

A two-stage heat treatment procedure was therefore developed which avoided spattering of the mixture, achieved good alloy homogeneity, and kept the vaporization losses to a safe minimum. In the first stage, it was discovered that the manner in which the initial metals were arranged in the nickel boat had great influence upon the spattering of the mixture. To reduce the spattering, the sodium and potassium metals were rolled into very thin sheets and placed in the boat in successive layers with antimony powder between them so that they had the appearance of a multiple sandwich.

During this first stage, once the nickel boat was in proper position inside the furnace , the temperature of the furnace was raised very slowly, at a rate of 50°C per hour up to 150°C. When the 150°C temperature was reached, the power supply of the furnace was turned off, and the furnace was cooled to room temperature. The nickel boat was moved by the steel rod to the original position inside the Tygon tubing. The tubing containing the nickel boat was then clamped on both ends, removed from the furnace setup, and transferred to the dry box.

In the dry box the sintered alloy was removed from the nickel boat, crushed into a fine powder in an agate mortar, and mixed thoroughly. This powder was then returned to the nickel boat for replacement in the tubing. Subsequently, the tubing was removed from the dry box and again transferred to the furnace setup in the same manner as described previously.

The second heat treatment of the alloy was performed in a manner different from that of the first. In this second stage, the temperature of the furnace was raised very rapidly to 700°C, requiring approximately 30 minutes, and then followed by a very slow cooling to 320°C at a rate of 50°C per hour. The 320°C temperature was held constant for about 8 hours. Cooling of the furnace to room temperature at a rate of 50°C per hour followed. Once the alloy reached room temperature, it was pulled to the proper position in the Tygon tubing by the steel rod; the tubing was clamped on both ends and, as described before, transferred to the dry box.

Alloys having more than 50 at. % Sb showed nickel pick-up from the boat during the second heat treatment. When this discovery was made, the procedure was changed. Thereafter, those alloys rich in antimony were held at a temperature of 450°C as a maximum instead of the 700°C temperature used for the rest of the alloys. In this way the alloys rich in antimony did not attack the nickel boat. Alloys having less than 40 at. % Sb did not show nickel pick-up and could safely be treated at temperatures higher than 450°C.* The nickel pick-up is explained by the fact that alloys having more than 50 at. % Sb have free antimony, which, of course, tends to react with the nickel of the boat and thereby decrease its free energy. This is an expected spontaneous process since the nickel-antimony compound produced is more stable than free antimony.

Alloys having less antimony than 25 at. % did not react so violently and did not produce spattering. Therefore, they did not need to be heat treated in two stages. To avoid appreciable volatilization losses (sodium, potassium, or sodium-potassium phases were present), the temperature for the heat treatment of these alloys was limited to 300°C. This temperature was held for 1 hour, and then the alloy was cooled to room temperature at a rate of 50°C per hour.

After the heat treatment, the alloy weight was checked against the charge weight. Serious weight losses were a basis for alloy rejection. Negligible weight losses indicated that the true composition was therefore close to the intended value.

* Nickel is practically insoluble in sodium and potassium below the boiling temperatures of these two alkali metals (12).

Preparation of Alloy Specimens for X-ray Diffraction Analysis. Powder samples for X-ray diffraction examination were prepared under nitrogen atmosphere in the dry box; the specimens were protected during X-ray analysis by enclosing them in thin-wall pyrex capillary tubes. First, portions of the alloys were cut off and crushed in an agate mortar under dry paraffin oil; the resulting sludge was drawn by capillary action into the dry 0.3-mm pyrex capillary tubes.

The atmosphere within the dry box showed little tendency to attack samples of alloys rich in antimony, but alloys having greater alkali content than 50 at. % were attacked rapidly enough to cause oxidation. For this reason it was necessary to keep the crushed or powdered material immersed in paraffin oil. The paraffin oil had been dried by shaking it with a liquid sodium-potassium alloy in a flask to disperse the alloy. Under these conditions the powder photographs indicated no decomposition into alkali oxides and metallic antimony, whereas the photographs taken of specimens prepared in the dry nitrogen atmosphere alone showed decomposition.

Earlier powder photographs taken of material which was powdered under paraffin oil in the presence of room air and then drawn into capillary tubes showed substantial decomposition into metallic antimony and alkali oxides.

The thin-wall pyrex capillary tubes used in the X-ray work were hand drawn over a flame. Only the thinnest walled and smallest external diameter tubes (less than 0.5 mm) were selected. These were then placed within larger pyrex test tubes which were then evacuated and sealed off to be later opened in the dry box.

Before the capillaries containing the alloys were removed from the dry box, their ends were sealed with paraffin wax and coated with Duco cement.*

X-ray analysis was performed by the standard powder diffraction method at room temperature. The most suitable exposure time was 8 hours at a current of 18 milliamperes, and 50 kilovolts.

Melting Temperature Determination Procedure. The melting temperature determinations of the newly discovered phases were made by classical thermal analysis methods.

The tests were performed using the previously prepared alloys. Approximately 30 grams of each corresponding alloy was ground inside the dry box and placed in a Vycor crucible. The crucible was then inserted into a one-end closed mullite tube. A rubber stopper containing connections for the argon gas circulation and the thermocouple was then inserted securely into the open end of the mullite tube. The Tygon tubing was clamped before the mullite tube was transferred from the dry box to the crucible furnace. The ends of the Tygon tubing leading from the mullite tube were then connected to the gas purification train and the oil bubbler, as shown in Fig. 8.

Thereafter, the system was evacuated in the same manner as described earlier for the preparation of alloys for phase relationship determinations. The purified argon gas was allowed to enter and fill

* Earlier powder photographs showed several degrees of decomposition. Evidently the wax seal alone was imperfect, as the powder decomposed gradually, proving useless after one day.

the system until inside pressure equaled the atmospheric. At this stage, the clamps from the Tygon tubing were released to permit the argon gas to fill the mullite tube. Subsequently, the gas passed through the oil bubbler trap, and was finally exhausted to the atmosphere.

The power supply to the furnace was then turned on, and the temperature of the system was raised slowly to approximately 50°C above the temperature at which the alloy melted. The melting temperature was approximately obtained at the moment the thermocouple sunk into the melting alloy (the thermocouple being pressed continuously under slight hand pressure).

Once the temperature of the system was stabilized near 50°C above the melting temperature, the reduction-geared motor operating the Variac transformer of the furnace was turned on and the temperature of the furnace was reduced continuously at a rate of approximately 2°C per minute. Recording of the temperature was made every minute and the results plotted to obtain the temperature-time cooling curve and the arrest temperature.

EXPERIMENTAL RESULTS AND DISCUSSION

For convenience, the experimental results and discussion are separated into five sections: binary sodium-potassium system, binary sodium-antimony system, binary potassium-antimony, ternary sodium-potassium-antimony system, and melting temperature determinations of the new phases found in this study.

Binary Sodium-Potassium System

The author considered that this phase diagram seemed well established, as summarized by Hansen, and especially by the thorough examination of MacDonald, Pearson and Towle (15), so that no further investigation was deemed necessary.

Previous thermal analysis work on the Na-K binary alloy series by van Rossen Hoogendijk (16), Jänecke (17), and Rinck (18) had indicated zero solid solubility at each limit (100% Na, 100% K), but studies of MacDonald proved, by electrical resistivity measurements, that solubility entends a few per cent from either limit.

MacDonald and co-workers (15) re-examined this system very carefully. They made a rather extended series of measurements of the electrical resistance of potassium-sodium alloys, which enabled them to construct an equilibrium diagram for this binary system in considerably more detail than had previously been available. Except for small modifications and terminal solid solubilities, their phase diagram agrees with that developed by the previous investigators.

Here, the author would like to mention the advantages of measuring resistance versus temperature as a method of studying alloy systems. This method requires a small amount of alloy, and the only necessary measurements are on alloys which are strictly in equilibrium when in the vicinity of phase boundaries. These boundaries can be located, if necessary, in a rapid preliminary survey. By contrast, thermal analysis involves problems of establishing steady heating or cooling rates and does not generally permit measurements to be made on alloys annealed exactly to equilibrium at a particular temperature.

Binary Sodium-Antimony System

The Na-Sb phase diagram had been determined by Mathewson (1) and was apparently well established. The diagram, in the range 50 to 100 atomic % Sb, was verified roentgenographically by Zintl and Dullenkopf (4).

The author verified the phase relationships present at room temperature in this alloy series by making seven alloy compositions and studying the corresponding X-ray diffraction photographs by standard procedures. Table 1 shows the compositions made and the results obtained.

TABLE 1

Alloy Compositions Prepared in the Binary Sodium-Antimony System

Alloy Number	Alloy Composition, Weight % Na	Sb	Phases Present
1	51.7	48.3	Na - Na_3Sb
2	37.0	63.0	Na_3Sb
3	26.0	74.0	Na_3Sb - NaSb
4	22.1	77.9	Na_3Sb - NaSb
5	16.0	84.0	NaSb
6	3.0	97.0	NaSb - Sb
7	1.9	98.1	NaSb - Sb

The X-ray powder photograph obtained for Na_3Sb was compared with that available in the A.S.T.M. Powder Data File, and is presented in Appendix III. Although the NaSb compound was known, no record of the powder pattern was given in the literature. The powder pattern obtained in this study for NaSb is listed in Appendix III.

There were no noticeable shifts in the line positions of the powder photographs obtained in this study. Therefore, the compounds can be considered stoichiometric, and the solid solubilities may be regarded as negligible. These results were expected to occur since the crystal structures of the intermetallic compounds differ markedly from those of the end elements, which, in turn, differ widely from each other. Also, antimony differs radically from sodium in chemical nature and atomic diameter.

Complete insolubility of any component in any phase at equilibrium is apparently a thermodynamic impossibility (20). Whenever two phases coexist at equilibrium in a binary alloy, the composition of each must vary in a predictable manner if the temperature of the alloy is changed. Obviously, the composition of a pure element cannot vary. The only possible conclusion is that the two phases present can never be pure. They must actually be solutions, and the extent of solubility of each component within the other must vary continuously with the temperature of the system. This does not mean that the solubility of each component within the other is necessarily extensive or even detectable by ordinary means. Cases are known in which only the most precise analytical techniques are capable of detecting the minute amount of the solute element dissolved at saturation.

If only one phase is present in a binary alloy at equilibrium, $f = 2$ ($f = c - p + 2$; where f = degrees of freedom, c = components and p = phases). The two degrees of freedom are evidently concentration and temperature. It is somewhat confusing to consider concentration as a possible variable in a one-phase system, since the composition of the single phase that makes up the system could vary only if the overall composition of the alloy were changed, and this is obviously impossible in an isolated system. However, the phase rule is directly concerned only with the number of components present in a system, and not with their total or relative amounts. The fact that in this case $c = 2$ and $p = 1$ indicates that the single phase being considered is either a

liquid solution or a solid solution. The fact that concentration exists as a degree of freedom indicates simply that this liquid or solid solution is unsaturated; it is capable of dissolving an additional amount of either of its components, even though another condition of the system which is not considered by the phase rule makes such an addition impossible. A one-phase binary alloy is, then, always an unsaturated solution which can be heated or cooled freely over an appreciable range of temperatures without undergoing any other significant change.

Therefore, the phase rule implicitly requires that all the phases appearing in a binary alloy series be solutions (20). This rule applies to intermetallic compounds as well as terminal solid solutions.

The alloys of the alkali metals with antimony represent borderline cases between metallic alloys and ionic crystals, as is evidenced by the heat of formation, per gram atom of alloy at 298°K, of the alkali antimonides: -17,850 cal., -11,800 cal., and -7,900 cal. for K_3Sb, Na_3Sb and NaSb respectively (19). These values indicate the strength of the atomic bonds in these intermetallic compounds. The stability of these phases is also evidenced by the fact that their melting temperatures are high despite the large atomic proportion of alkali metal. This is particularly true concerning the compound of the form M_3Sb (where M is any alkali metal).

Several characteristics concerning the intermetallic compounds in this alloy series are listed in Appendix IV.

Binary Potassium-Antimony System

Twenty-one alloy compositions were prepared to verify the phase relationships present at room temperature in the K-Sb binary system. The X-ray diffraction photographs were studied by standard procedures. Table 2 shows the compositions made and the results obtained.

The study by the author of the phase relationship of this system at room temperature proved that Parravano (2) overlooked two compounds. As pointed out in the Literature Survey, the phase diagram shows the presence of two congruent compounds: K_3Sb and KSb. The two new compounds are proposed as having the compositions K_5Sb_4 and KSb_2.

TABLE 2

Alloy Compositions Prepared in the Binary Potassium-Antimony System

Alloy Number	Alloy Composition, Weight % K	Sb	Phases Present
8	7.5	92.5	Sb - KSb_2
9	9.7	90.3	Sb - KSb_2
10	14.0	86.0	KSb_2
11	14.2	85.8	KSb_2 - KSb
12	14.7	85.3	KSb_2 - KSb
13	18.2	81.8	KSb_2 - KSb
14	20.8	79.2	KSb_2 - KSb
15	21.9	78.1	KSb_2 - KSb

TABLE 2 (Con't)

Alloy Compositions Prepared in the Binary Potassium-Antimony System

Alloy Number	Alloy Composition, Weight % K	Sb	Phases Present
16	24.0	76.0	KSb
17	26.0	74.0	KSb - K_5Sb_4
18	27.4	72.6	KSb - K_5Sb_4
19	28.7	71.3	K_5Sb_4
20	29.0	71.0	K_5Sb_4 - K_3Sb
21	29.9	70.1	K_5Sb_4 - K_3Sb
22	31.6	68.4	K_5Sb_4 - K_3Sb
23	35.4	64.6	K_5Sb_4 - K_3Sb
24	39.5	60.5	K_5Sb_4 - K_3Sb
25	44.0	56.0	K_5Sb_4 - K_3Sb
26	47.7	52.3	K_5Sb_4 - K_3Sb
27	49.0	51.0	K_3Sb
28	64.5	35.5	K_3Sb - K

The K_3Sb powder pattern obtained in this study was compared with the available data in the A.S.T.M. Powder Data File and is listed in Appendix III. No X-ray powder pattern data were available in the literature for KSb. The data obtained in this study are given in Appendix III. The X-ray powder patterns data of the new phases KSb_2 and K_5Sb_4 are given in Appendix III. There were no noticeable shifts of line positions in the powder photographs. Therefore, the compounds can be considered to be stoichiometric, and the solid solubilities may be regarded as negligible.

Several characteristics of the single phases in this alloy series are listed in Appendix IV.

Discussion of the New Phases Found in the Potassium-Antimony System

From the obtained results, it appears that in the alloy series of antimony with the alkali metals, the greater the atomic weight of the alkali metal, the greater the number of intermetallic compounds in the corresponding alloy series. Consequently, lithium produces only one compound, Li_3Sb; sodium produces two, Na_3Sb and NaSb; potassium produces K_3Sb and KSb, and the proposed K_5Sb_4 and KSb_2. The Cs-Sb phase diagram is not complete. It shows the Cs_3Sb compound only, but is expected to produce at least the same number of compounds as potassium. This can be anticipated if we consider the fact that antimony has an atomic radius of 2.90 A.U., and the atomic radius of the alkali increase from 3.03 A.U. in lithium to 5.31 A.U. in cesium. Therefore, we could expect that the greater the atom radius of the alkali metal, the probabilities for different atomic arrangements also increase in the alloy series with antimony.

In addition, because of the strain involved in the formation of K_3Sb, the compound K_5Sb_4 is expected in the K-Sb system since this arrangement releases some of the stress involved in the K_3Sb coordination. For the same reason, alkaline metals with higher atomic number than potassium -- such as rubidium and cesium -- are expected to form a M_5Sb_4 type of compound (and possibly some others in the range M_5Sb to M_3Sb).

As will be seen later in the discussion of the ternary Na-K-Sb system, sodium substitutes for potassium in the K_3Sb compound, along the pseudo-binary Na_3Sb-K_3Sb line, relieving the stresses until finally stability is achieved at the NaK_2Sb composition.

A further evidence of the strain involved in the formation of K_3Sb is the large heat of formation at 298°K: -17,850 cal/g - atom of alloy (19) as compared with -11,800 cal/g - atom of alloy for Na_3Sb.

The tendency of any phase to undercool seems, in general, to increase in rough proportion to the complexity of its crystal structure. The results, when undercooling is extreme, are sometimes quite surprising when occurring in an eutectic-type alloy. Undercooling tends to shift the eutectic point toward a lower temperature and toward a higher content of the phase which undercools more. Undercooling is frequently very evident in eutectic-type alloys in which one of the phases is a compound. However, a far more extreme case of undercooling has been noted in several alloy series containing intermetallic compounds, in which, by rapid cooling, a compound normally present can be completely prevented from appearing. This could have happened very easily to Parravano in his study on the binary K-Sb system, explaining the reason for his not noticing the compound K_5Sb_4. This seems to be most common when the compound in question forms peritectically, but it occurs also in compounds that freeze normally (20).

The KSb_2 phase was also overlooked by Parravano (2). He studied the K-Sb system by microscopic procedures and missed the KSb_2 phase.

This is easily understandable considering that KSb_2 and KSb are difficult to differentiate under the microscope because of their similarities.

Ternary Sodium-Potassium-Antimony System

The Na-K-Sb ternary system has been studied in this investigation by X-ray diffraction methods. The results are presented in the form of an isothermal section at room temperature. To draw this isothermal section of the Na-K-Sb diagram, 61 ternary Na-K-Sb compositions were prepared. The alloys and X-ray specimens were prepared as described previously under Experimental Apparatus and Procedure. The corresponding X-ray powder patterns were studied by the conventional method and were the basis for evaluation of the Alkemade triangles. Table 3 shows the compositions made and the results obtained.

TABLE 3

Alloy Compositions Prepared in the Ternary Sodium-Potassium-Antimony System

Alloy Number	Alloy Composition, Weight %			Phases Present
	Na	K	Sb	
29	8.5	6.5	85.0	NaSb - KSb_2
30	5.4	9.1	85.5	NaSb - KSb_2
31	1.0	13.1	85.9	NaSb - KSb_2
32	3.8	4.9	91.3	NaSb - Sb - KSb_2
33	1.1	3.6	95.3	NaSb - Sb - KSb_2
34	10.0	9.0	81.0	NaSb - KSb

TABLE 3 (Con't)

Alloy Compositions Prepared in the Ternary Sodium-Potassium-Antimony System

Alloy Number	Alloy Composition, Weight % Na	K	Sb	Phases Present
35	7.6	12.8	79.6	NaSb - KSb
36	12.5	5.4	82.1	NaSb - KSb_2 - KSb
37	4.4	13.2	82.4	NaSb - KSb_2 - KSb
38	12.7	10.8	76.5	NaSb - KSb - Na_3Sb
39	17.0	12.9	70.1	Na_3Sb - KSb
40	13.4	15.3	71.3	Na_3Sb - KSb
41	29.0	9.8	61.2	Na_3Sb - Na_2KSb
42	22.2	18.9	58.9	Na_2KSb
43	8.8	22.2	69.0	Na_2KSb - KSb
44	14.0	17.1	68.9	Na_2KSb - Na_3Sb - KSb
45	20.4	19.9	59.7	Na_2KSb - KSb - NaK_2Sb
46	7.9	26.1	66.0	Na_2KSb - KSb - NaK_2Sb
47	21.2	20.4	58.4	Na_2KSb - NaK_2Sb
48	17.3	25.7	57.0	Na_2KSb - NaK_2Sb
49	16.0	27.4	56.6	Na_2KSb - NaK_2Sb
50	11.2	34.0	54.8	Na_2KSb - NaK_2Sb
51	54.7	17.5	27.8	Na_2KSb - NaK_2Sb
52	10.4	35.1	54.5	NaK_2Sb
53	9.6	33.3	57.1	NaK_2Sb - Na_2KSb - KSb

TABLE 3 (Con't)

Alloy Compositions Prepared in the Ternary Sodium-Potassium-Antimony System

Alloy Number	Alloy Composition, Weight % Na	K	Sb	Phases Present
54	6.7	31.2	62.1	NaK_2Sb - KSb
55	4.3	28.7	67.0	NaK_2Sb - KSb
56	2.3	30.0	67.7	NaK_2Sb - K_5Sb_4
57	4.8	30.3	64.9	NaK_2Sb - KSb - K_5Sb_4
58	3.1	28.9	68.0	NaK_2Sb - KSb - K_5Sb_4
59	2.2	27.4	70.4	NaK_2Sb - KSb - K_5Sb_4
60	7.0	39.5	53.5	α
61	5.7	39.9	54.4	α - K_5Sb_4
62	5.0	42.3	52.7	α
63	1.9	45.1	53.0	α - K_5Sb_4
64	1.5	45.6	52.9	α - K_5Sb_4
65	0.8	46.7	52.5	α - K_5Sb_4
66	1.3	32.5	66.2	α - K_5Sb_4
67	0.3	33.0	66.7	α - K_5Sb_4
68	0.5	36.6	62.9	α - K_5Sb_4
69	42.0	14.5	43.5	Na_3Sb - Liq.
70	42.7	6.7	50.6	Na_3Sb - Liq. - Na
71	53.9	7.8	38.3	Na_3Sb - Liq. - Na
72	53.3	11.4	35.3	Na_3Sb - Liq. - Na
73	18.1	53.0	28.9	Na_2KSb - Liq.
74	30.0	17.0	53.0	Na_3Sb - Na_2KSb - Liq.
75	40.0	14.6	45.4	Na_3Sb - Na_2KSb - Liq.
76	37.7	20.0	43.3	Na_3Sb - Na_2KSb - Liq.
77	33.0	23.4	43.6	Na_3Sb - Na_2KSb - Liq.
78	21.6	44.1	34.3	Na_2KSb - K - Liq.

TABLE 3 (Con't)

Alloy Compositions Prepared in the Ternary Sodium-Potassium-Antimony System

Alloy Number	Alloy Composition, Weight % Na	K	Sb	Phases Present
79	12.0	56.7	31.3	Na_2KSb - K
80	20.4	24.6	55.0	Na_2KSb - NaK_2Sb - K
81	18.1	29.2	52.7	Na_2KSb - NaK_2Sb - K
82	9.4	57.3	33.3	Na_2KSb - NaK_2Sb - K
83	10.2	60.0	29.8	Na_2KSb - NaK_2Sb - K
84	7.1	55.7	37.2	NaK_2Sb - K
85	4.9	68.5	26.6	NaK_2Sb - K
86	5.2	50.9	43.9	α - K
87	4.6	58.8	36.6	α - K
88	0.9	63.4	35.7	α - K
89	0.5	73.6	25.9	α - K

In the ternary Na-K-Sb system, Fig. 10, are twelve Alkemade triangles and two three-component compounds: Na_2KSb previously found by Sommer (3) and the new compound K_2NaSb. The powder pattern of K_2NaSb has the same general appearance as those of Na_3Sb and K_3Sb, and is expected to have the same crystal structure (i.e. hexagonal Na_3As type). Unlimited solid solubility exists between K_2NaSb and K_3Sb. (This solid solution will hereafter be designated as the α phase). Consequently, the Alkemade triangles K_5Sb_4-K_3Sb-K_2NaSb and K_3Sb-K_2NaSb-K cover portions of two-phase regions.

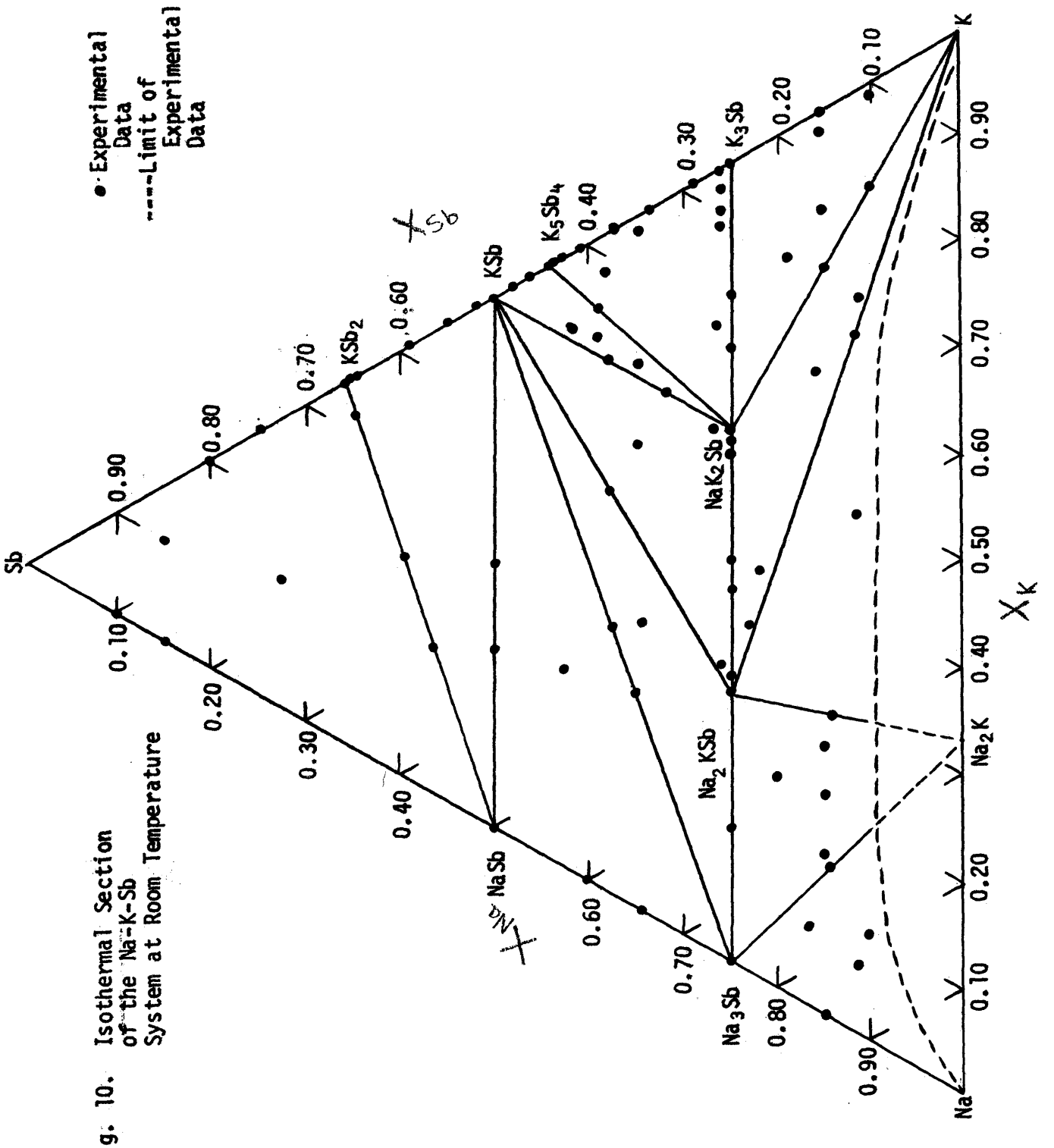

Fig. 10. Isothermal Section of the Na-K-Sb System at Room Temperature

Several characteristics of the two ternary phases are listed in Appendix IV.

Aside from the above-mentioned solid solution, no other clear line shifting of the powder photographs was observed, and the stability range of all the different phases was found to be very restricted. Very small deviations from their stoichiometric compositions cause precipitation of other phases.

The relative low atomic scattering power of the alkali metals involved, especially sodium (the average scattering power ratios of antimony, potassium and sodium are about 6:2:1) was a factor that contributed to the low intensity of the reflections. Some phases, especially KSb_2 and KSb, did not give sufficiently sharp reflections, and their X-ray powder patterns also proved rich in lines.

The high background intensity of the X-ray photographs was a characteristic in some of the alloy series studied. Practically all photographs show the high Bragg's angle reflections obscured by the high background intensity. This made the study of the binary and ternary alloy series involved in this work by X-ray powder methods quite difficult. The alternative of using the diffractometer was considered, but no suitable procedure could be successfully developed to keep the X-ray specimens from oxidation and decomposition.

Other factors that contributed to the high background intensity of the X-ray photographs were the paraffin oil used to protect the specimens against oxidation, the pyrex capillary tube wall enclosing the powder specimens, and the incoherent scattering due to the sample itself (especially that of sodium, because of its relatively low atomic weight).

To reduce these difficulties, minimum amounts of paraffin oil were used in the preparation of the X-ray specimens. The pyrex capillary tubes to be used as specimen holders were carefully checked; only very small diameters (less than 0.5 mm) and the thinnest-walled tubes possible were selected.

Several X-ray specimens were prepared from each alloy composition. Only the best specimens were chosen for exposure in the X-ray camera so that the clearest possible photographs could be obtained.

The powder patterns obtained for the end members of this ternary phase diagram, i.e. sodium, potassium and antimony, were compared with those available in the A.S.T.M. cards and are listed in Appendix III. The powder pattern for Na_2KSb obtained in this work and compared with the data obtained by (10) is also given in Appendix III. In addition, Appendix III shows the pattern obtained for the new ternary compound NaK_2Sb.

Alloys involving the K_5Sb_4 phase required longer homogenization than the others. If alloys involving the K_5Sb_4 phase were cooled from 700°C to 320°C faster than the established cooling rate, 50°C per hour, they did not reach equilibrium. These alloys then remained in metastable condition.

The alkali content of the alloys prepared in this investigation was limited to 90 atomic % (Na + K). Alloys having higher alkali content could not be heat treated and homogenized at the necessary temperatures without avoiding high degrees of oxidation. Also, alloys in

equilibrium with high proportions of liquid phase at room temperature (in the alkali rich region of the diagram) were difficult to sample.

Even though the alkali metals oxidize at very low oxygen pressures, the protective atmosphere used during the heat treatment of the alloys (purified argon gas) proved satisfactory in the range of alloy composition studied. The X-ray diffraction patterns were free from oxide lines.

The volatilization losses of the alloys during the heat treatment were small and were therefore neglected. The final compositions of the alloys were assumed to be that of the original mixture and therefore no chemical analysis of the final compositions was necessary.

Both the success in using the purified argon gas as a protective atmosphere during the heat treatment of the alloys, and the negligible vaporization losses of the alloys in the same process (even though they were heat treated at relatively high temperatures, close to the boiling temperatures of the alkali metals), can be attributed to the great negative deviation of the activity coefficient of the alkali metals when alloyed with antimony. Antimony decreases the activity coefficient of the alkali metals tremendously, as expected from the position of the metals in the periodic table. A further thermodynamic explanation is given in Appendix V.

Melting Temperature Determinations of the New Phases Found in this Study

The melting temperature determinations of the newly discovered phases were obtained by thermal analysis methods.

Structural changes in metals and alloys are accompanied by the evolution or absorption of latent heat of transformation, such as latent heat of fusion observed when a metal melts. It follows, therefore, that if a metal or alloy is heated or cooled under uniform conditions, the structural change will produce a bend in a time-temperature curve, and under suitable experimental conditions the temperature at which the inflection occurs will indicate the temperature at which the structural change takes place.

When a specimen is heated or cooled in a furnace, the rate at which the temperature of the specimen alters depends on the interchange of heat between the furnace and the specimen, and the rate at which the power supply of the furnace is increased or reduced.

After extensive testing in this investigation, it was determined that the cooling rates of the alloys were critical, and in order to obtain clear arrests in the curves the cooling rates had to be held to a minimum. The minimum cooling rate attainable with the setup at hand was approximately 2°C per minute.

Vycor crucibles were used to hold the alloys, after experiencing unsuccessful results with nickel crucibles. The use of nickel crucibles was discarded when it was discovered that nickel crucibles had the disadvantage of having high thermal conductivity, which masked the weak thermal arrests.

The cooling curves of all the intermetallic compounds studied, except K_5Sb_4, showed horizontal arrests typical of alloys that freeze at

constant temperature, indicating that these phases had congruent melting temperatures. In the case of K_5Sb_4, the corresponding cooling curve showed an arrest typical of alloys that solidify in a temperature range indicating an incongruent melting temperature.

The melting temperatures of the new phases found in this study are summarized as follows: 667°C for Na_2KSb; 618°C for NaK_2Sb; 509°C for K_5Sb_4 and 409°C for KSb_2.

SUMMARY AND CONCLUSIONS

The ternary sodium-potassium-antimony phase diagram has been investigated by X-ray diffraction techniques. The results are presented in the form of an isothermal section at room temperature, showing the tie-lines between the phases involved and the Alkemade triangles (Fig. 10).

The isothermal section of this phase diagram at room temperature shows 12 Alkemade triangles. The internal compound, Na_2KSb found by previous investigators, has been verified. A new ternary compound having the composition corresponding to the formula NaK_2Sb has been found. The compounds K_3Sb and NaK_2Sb show unlimited solid solubility, giving as a result two two-phase regions inside the diagram bounded by the triangles K_5Sb_4-NaK_2Sb-K_3Sb and K_3Sb-NaK_2Sb-K, respectively.

The binary sodium-antimony phase diagram developed by the previous investigator has been checked and verified by X-ray methods.

The binary potassium-antimony phase diagram investigated in this study showed two new compounds, KSb_2 and K_5Sb_4, which had been overlooked by the previous investigator.

It is of interest to note the stoichiometric nature of the intermetallic phases involved in this study. Aside from the above-mentioned solid solution, the X-ray powder diffraction photographs do not show other noticeable shifts in lines. The intermetallic compounds show a narrow range of stability, and small deviations from stoichiometry cause precipitation of other adjacent phases.

The "d" spacings for the phases involved in this study have been calculated from their corresponding powder diffraction photographs, and are listed in Appendix III.

High background intensity was a characteristic of most of the phases involved in this study. Also, the X-ray powder photographs of some of the phases proved rich in lines. Generally high-angle diffraction lines were obscured by the background intensity.

The fact that X-ray powder diffraction photographs were free of oxide lines proved that the experimental apparatus and procedure as established were satisfactory.

The reaction of alkali metals with antimony proved to be extremely exothermic, giving evidence of the strength of the bonds involved. In addition, the intermetallic compounds formed by alkali metals and elements of the V-A group show relative high melting temperatures despite the alkali content of the corresponding phases, proving that these alloys are borderline cases between ionic and metallic crystals.

Vaporization losses during the tests were small and considered negligible, due to the high negative deviation of the activity coefficient of the alkali metals in alloys with elements of the V-A group of the periodic table.

It may be concluded that in the alkali metal-antimony alloys, the greater the atomic number of the alkali metal involved, the greater will be the number of intermetallic phases in the corresponding binary diagram. This fact must be considered in future determination studies involving the alkali metal-antimony systems that remain incomplete at this time.

The melting temperatures of the new phases found in this study were determined by thermal analysis techniques. Na_2KSb melts congruently at 667°C; NaK_2Sb melts congruently at 618°C; K_5Sb_4 melts incongruently at 509°C; and KSb_2 melts congruently at 409°C.

APPENDIX I

Purity of Materials

Sodium (reagent, A.C.S.) cast into spheres and potassium (reagent, A.C.S.) cast into sticks were obtained from Matheson Coleman & Bell, a Division of the Matheson Company, Inc. of Norwood (Cincinnati), Ohio. The chemical analysis received from the supplier is shown below in weight percents:

Chloride (Cl)	-0.0015%
Heavy Metals (as Pb)	-0.0005%
Iron (Fe)	-0.001%
Nitrogen (N)	-0.003%
Phosphate (PO_4)	-0.0005%
Sulfate (SO_4)	-0.002%

By difference, the nominal sodium and potassium content were 99.9915 + %.

An antimony bar (high purity metal, 99.99 + %Sb) used in these experiments was supplied by American Smelting and Refining Company.

The argon gas used during the preparation of the alloys was obtained from the Linde Company, a Division of Union Carbide Corporation. The argon gas was reported by the manufacturer to be 99.995% argon, and dry.

The high purity dry nitrogen gas was also supplied by the Linde Company.

APPENDIX II

Oxygen Partial Pressures in Argon Gas During Purification

The alkali metals are very reactive and the oxygen partial pressure in equilibrium with the alkali metal - alkali oxide system is relatively small. This fact can be better visualized if potassium is used as an example:

$$4K_{(l)} + O_{2(g)} = 2K_2O_{(s)}$$

The partial pressure of oxygen in thermodynamic equilibrium in the $K\text{-}K_2O$ system can be estimated with the help of the thermodynamic equilibrium constant K, and the change in free energy ΔG° for the reaction. Using the following equations,

$$\log K = -\frac{\Delta G^\circ}{4.575 \times T}$$

and

$$K = \frac{(a_{K_2O})^2}{(a_K)^4 \times p_{O_2}}$$

several oxygen partial pressures in equilibrium with the system $K\text{-}K_2O$ have been calculated and are listed in the following Table 1. The activities of K and K_2O have been taken as one.

The free energy data has been taken from reference (21) unless otherwise stated.

TABLE 1

Oxygen Partial Pressure in Equilibrium in the K-K_2O System

Temperature, °C	ΔG°_T	$\log_{10} K$	p_{O_2}, atm.
100	-178,000	104.0	1.0×10^{-104}
300	-164,000	62.7	2.0×10^{-63}
500	-151,000	42.5	3.2×10^{-43}
700	-137,000	30.8	1.6×10^{-31}

It is obvious that the oxygen partial pressure in equilibrium with alkali metal - alkali oxide systems is relatively minute. In practice, however, the time necessary to reach equilibrium is longer at relatively low temperatures. Also, diffusion of oxygen decreases as the oxide layer builds up.

As mentioned before in Experimental Apparatus and Procedure, copper and titanium were used to purify the argon gas. The most probable reactions, during this purification step, at low oxygen content are:

$$4\ Cu_{(s)} + O_{2\,(g)} = 2\ Cu_2O_{(s)}$$

and $$2\ Ti_{(s)} + O_{2\,(g)} = 2\ TiO_{(s)}.$$

The free energy for the reactions are: $\Delta G^\circ_{900^\circ C}$ = -46,400 cal. and $\Delta G^\circ_{900^\circ C}$ = -194,600 cal. respectively. The oxygen partial pressures in equilibrium for the reactions are 1.4×10^{-10} atm. and 6.2×10^{-37} atm. respectively, indicating that oxygen in the argon gas leaving the

purification train should have an oxygen pressure of around 10^{-30} atm. This value is greater than the oxygen pressures obtained for the K-K_2O system and still the argon gas was a sufficient protective atmosphere during the tests.

A thermodynamic explanation for the use of this purified argon gas as protective atmosphere is given in Appendix V.

APPENDIX III

X-ray Powder Diffraction Data

The X-ray powder diffraction data of the phases involved in the present study are compiled in this appendix. If X-ray data was available in the literature for a given phase, it has been compared with that obtained in this investigation.

1. Na

X-ray Data Obtained in Present Study Compared with A.S.T.M. Powder Diffraction Data

Present Study Data		A.S.T.M. Data	
d spacing (A.U.)	Observed Relative Intensity	d spacing (A.U.)	Relative Intensity
3.036	vs	3.02	100
2.145	s	2.13	15
1.752	s	1.75	20
1.516	m	1.51	5
1.357	m	1.36	5
1.238	vw	1.25	3
1.146	w	1.15	3
1.009	vw	-	-
.957	vw	-	-
.912	vw	-	-
.874	vw	-	-
.840	vw	-	-

2. K

X-ray Data Obtained in Present Study Compared with A.S.T.M. Powder Diffraction Data

Present Study Data		A.S.T.M. Data	
d spacing (A.U.)	Observed Relative Intensity	d spacing (A.U.)	Relative Intensity
3.761	vs	3.75	100
2.665	s	2.65	16
2.171	s	2.16	30
1.880	m	1.87	4
1.682	m	1.68	4
1.518	vw	1.52	2
1.430	w	1.42	2
1.250	vw	-	-

3. Sb

X-ray Data Obtained in Present Study Compared with A.S.T.M. Powder Diffraction Data

Present Study Data		A.S.T.M. Data	
d spacing (A.U.)	Observed Relative Intensity	d spacing (A.U.)	Relative Intensity
3.752	vw	3.753	25
-	-	3.538	4
3.109	vs	3.109	100
2.249	s	2.248	70
2.151	s	2.152	56
1.929	w	1.929	12
1.878	w	1.878	35
1.771	s	1.770	26
1.556	s	1.555	15
1.480	w	1.479	13
1.437	vw	1.437	12
1.416	s	1.416	63
1.367	s	1.368	67
1.319	vw	1.318	30
1.261	w	1.261	40
1.252	w	1.252	25
1.241	vw	1.243	30
1.218	vw	1.219	11
1.195	vw	1.195	12
1.180	vw	1.180	5
1.124	vw	1.124	12
1.083	w	1.083	32
-	-	1.079	16
1.077	w	1.077	12
1.060	vw	1.061	16
1.036	w	1.037	17
1.018	w	1.018	27
.997	vw	.997	25
.988	vw	.988	24
.971	w	.971	15
-	-	.965	8
-	-	.940	7
.934	vw	.934	13
.921	vw	.920	8
.899	vw	.898	10

4. Na_3Sb

X-ray Data Obtained in Present Study Compared with A.S.T.M. Powder Diffraction Data

Present Study Data		A.S.T.M. Data	
d spacing (A.U.)	Observed Relative Intensity	d spacing (A.U.)	Relative Intensity
4.746	s	4.75	57
4.634	s	4.65	50
4.176	vs	4.16	80
3.318	w	3.32	25
2.680	vs	2.67	100
2.615	vs	2.61	100
2.374	vw	2.38	32
2.332	s	2.33	80
2.254	m	2.26	57
2.112	vw	-	-
2.073	vw	-	-
1.870	s	1.87	75
1.777	m	1.78	57
1.756	m	1.76	50
1.725	m	1.73	60
1.658	vw	-	-
1.643	vw	-	-
1.584	w	1.59	35
1.546	m	1.55	45
1.533	s	1.54	75
1.498	vw	1.50	30
1.469	m	1.47	57
1.409	vw	1.41	18
1.362	m	1.37	60
1.338	vw	1.34	50

5. K_3Sb

X-ray Data Obtained in Present Study Compared with A.S.T.M. Powder Diffraction Data

Present Study Data		A.S.T.M. Data	
d spacing (A.U.)	Observed Relative Intensity	d spacing (A.U.)	Relative Intensity
5.377	s	5.31	55
5.259	s	-	-
4.710	s	4.70	70
3.033	vs	3.01	100
2.955	vs	2.95	100
2.687	vw	-	-
2.636	s	2.63	80
2.551	w	2.54	55
2.116	s	2.11	83
2.005	m	2.00	60
1.987	w	1.98	40
1.951	m	1.94	55
1.789	w	-	-
1.750	m	1.74	70
1.733	s	1.73	90
1.692	vw	-	-
1.662	m	1.66	55
1.539	m	1.51	70
1.513	w	1.51	55

6. KNa_2

A.S.T.M. X-ray Powder Diffraction Data

d spacing (A.U.)	Relative Intensity	h k l
3.70	70	110
3.43	70	103
3.17	100	200, 112, 201, 004
2.29	40	105, 212
2.15	50	300
2.10	50	213
2.04	40	302, 006
1.95	100	205, 106
1.91	30	214
1.87	70	220
1.72	50	215, 206
1.64	40	107, 206
1.60	40	401, 224
1.56	20	216, 402, 314, 207
1.49	40	108
1.42	40	410, 118
1.38	50	226, 412
1.35	40	405, 316
1.30	30	218, 500
1.27	20	325, 406, 502
1.25	20	317, 308, 330, 503
1.22	40	332, 421
1.16	20	318
1.13	20	505, 512, 424
1.10	40	425, 506
1.08	20	319, 600

7. NaSb

X-ray Powder Diffraction Data Obtained in Present Study

d spacing (A.U.)	Observed Relative Intensity	Line Diameter (cm)
6.000	m	2.575
5.530	s	2.795
4.613	s	3.355
4.170	vs	3.715
3.665	m	4.235
3.116	s	4.995
3.004	s	5.185
2.938	w	5.305
2.872	w	5.430
2.797	m	5.580
2.758	vw	5.660
2.649	vw	5.900
2.590	m	6.040
2.503	vw	6.255
2.405	m	6.520
2.310	w	6.800
2.234	s	7.040
2.164	m	7.280
2.118	m	7.445
2.087	w	7.560
2.048	m	7.710
2.031	vw	7.780
2.005	w	7.885
1.976	vw	8.010
1.930	vw	8.210
1.908	vw	8.310
1.877	vw	8.455
1.845	vw	8.615
1.779	w	8.955
1.750	w	9.115
1.713	vw	9.330
1.683	w	9.510
1.657	vw	9.665
1.632	vw	9.830
1.616	vw	9.935
1.582	w	10.170

7. NaSb (Con't)

X-ray Powder Diffraction Data Obtained in Present Study

d spacing (A.U.)	Observed Relative Intensity	Line Diameter (cm)
1.572	w	10.240
1.543	w	10.450
1.526	w	10.580
1.515	w	10.670
1.496	vw	10.825
1.479	vw	10.955
1.469	vw	11.035
1.447	vw	11.225
1.421	vw	11.455
1.410	vw	11.555
1.353	m	12.110
1.322	w	12.440
1.301	vw	12.675
1.279	w	12.925
1.257	w	13.190
1.239	vw	13.420
1.206	w	13.860

8. KSb

X-ray Powder Diffraction Data Obtained in Present Study

d spacing (A.U.)	Observed Relative Intensity	Line Diameter (cm)
6.502	s	2.375
6.058	m	2.550
5.852	m	2.640
4.981	m	3.105
4.580	s	3.380
4.462	m	3.460
4.026	m	3.850
3.343	s	4.650
3.250	vs	4.785
3.150	s	4.940
3.019	vs	5.160
2.943	vw	5.295
2.847	m	5.480
2.782	vw	5.610
2.707	vw	5.770
2.638	vs	5.925
2.539	vw	6.165
2.480	w	6.315
2.396	s	6.545
2.290	m	6.860
2.260	w	6.955
2.242	m	7.015
2.216	w	7.100
2.185	m	7.205
2.171	s	7.255
2.120	vw	7.435
2.099	w	7.515
2.050	vw	7.705
2.037	w	7.765
1.966	vw	8.050
1.942	vw	8.155
1.902	vw	8.335
1.893	vw	8.380
1.836	vw	8.660
1.819	vw	8.745
1.796	vw	8.865

8. KSb (Con't)

X-ray Powder Diffraction Data Obtained in Present Study

d spacing (A.U.)	Observed Relative Intensity	Line Diameter (cm)
1.754	vw	9.095
1.735	w	9.200
1.716	w	9.310
1.680	w	9.525
1.659	w	9.655
1.628	w	9.855

9. K_5Sb_4

X-ray Powder Diffraction Data Obtained in Present Study

d spacing (A.U.)	Observed Relative Intensity	Line Diameter (cm)
6.166	vw	2.505
5.942	w	2.600
5.841	vw	2.645
5.589	m	2.765
5.030	vw	3.075
4.872	vs	3.175
4.732	vw	3.270
4.399	vw	3.520
4.297	w	3.605
4.143	vw	3.740
3.635	vw	4.270
3.464	vw	4.485
3.298	s	4.715
3.254	s	4.780
3.065	m	5.080
2.773	s	5.630
2.737	vs	5.705
2.588	m	6.045
2.464	s	6.360
2.458	w	6.375
2.421	m	6.475
2.386	m	6.575
2.358	vw	6.655
2.315	w	6.785
2.237	m	7.030
2.179	vw	7.225
2.152	m	7.320
2.102	vw	7.505
2.071	m	7.620
2.038	m	7.750
2.006	vw	7.880
1.944	w	8.150
1.913	w	8.290
1.882	w	8.435
1.844	m	8.620
1.813	m	8.775
1.800	vw	8.845

9. K_5Sb_4 (Con't)

X-ray Powder Diffraction Data Obtained in Present Study

d spacing (A.U.)	Observed Relative Intensity	Line Diameter (cm)
1.746	w	9.140
1.736	w	9.195
1.664	m	9.625
1.654	w	9.690
1.638	w	9.790
1.616	vw	9.940
1.586	m	10.145
1.568	vw	10.270
1.556	vw	10.360
1.528	vw	10.570
1.506	w	10.740

10. KSb_2

X-ray Powder Diffraction Data Obtained in Present Study

d spacing (A.U.)	Observed Relative Intensity	Line Diameter (cm)
7.048	s	2.190
5.215	s	2.965
4.776	s	3.240
3.522	w	4.410
3.267	w	4.760
3.147	vs	4.945
3.048	s	5.110
2.938	vs	5.305
2.694	m	5.800
2.316	m	6.780
2.285	m	6.875
2.245	vw	7.005
2.176	m	7.235
2.151	vw	7.325
2.115	m	7.455
2.090	vw	7.550
2.056	w	7.680
2.031	m	7.780
1.958	vw	8.085
1.936	w	8.195
1.890	w	8.395
1.834	vw	8.670
1.819	vw	8.745
1.778	vw	8.960
1.762	w	9.050
1.737	w	9.190
1.674	w	9.560
1.634	vw	9.820
1.602	vw	10.030
1.577	m	10.205
1.554	w	10.370
1.521	vw	10.620
1.499	vw	10.795
1.473	w	11.005
1.413	vw	11.530
1.400	vw	11.655
1.362	w	12.025
1.353	w	12.115

11. Na_2KSb

X-ray Powder Diffraction Data Obtained in Present Study

d spacing (A.U.)	Observed Relative Intensity	h k l *
4.449	s	111
3.862	s	200
2.740	vs	220
2.333	s	311
2.231	m	222
1.932	m	400
1.773	m	331
1.728	m	420
1.578	s	422
1.487	m	511, 333
1.367	m	440
1.307	m	531
1.289	m	600, 442
1.223	m	620
1.179	w	533
1.166	w	622
1.118	w	444
1.083	w	711, 551
1.074	w	640
1.034	m	642
1.007	w	731, 553
.938	w	820, 644
.912	w	822, 660

* The pattern has been indexed on the basis of a cubic cell by means of the slide rule method and the quadratic forms of Miller indices available in Cullity's book, page 471. From the systematic absence of reflections with mixed odd and even indices it must be concluded that this compound possesses a face-centered cubic structure. These results agree with those obtained by Scheer and Zalm (10).

12. NaK_2Sb

X-ray Powder Diffraction Data Obtained in Present Study

d spacing (A.U.)	Observed Relative Intensity	Line Diameter (cm)
5.481	s	2.820
4.895	s	3.160
4.462	vs	3.470
2.922	vs	5.335
2.812	vs	5.550
2.502	s	6.260
2.434	w	6.440
2.382	m	6.585
2.028	s	7.790
1.998	m	7.915
1.963	m	8.065
1.839	vw	8.645
1.823	m	8.725
1.711	vw	9.340
1.644	s	9.750
1.622	m	9.895
1.555	w	10.365
1.531	s	10.545
1.490	vw	10.870
1.459	vw	11.120
1.408	m	11.580
1.398	w	11.675
1.363	w	12.015
1.339	w	12.255
1.317	vw	12.490
1.297	vw	12.720
1.266	s	13.075
1.251	w	13.265
1.231	w	13.510
1.213	m	13.765
1.191	w	14.055
1.181	m	14.205

APPENDIX IV

Characteristics of Intermetallic Compounds Involved in this Study

Na_3Sb - Has a bright metallic blue color. Does not show clear cleavage.

NaSb - Has a silvery color and shows good cleavage.

K_3Sb - Has a yellow-green color, shiny and iridescent. Does not show clear cleavage.

KSb - Has a silvery color. Needle-like and shows clear cleavage parallel to the needle axis.

KSb_2 - Has a silvery color, like KSb, but less shiny. Has a needle-like appearance, but the needles are longer and more flexible than those of KSb.

K_5Sb_4 - Has a dull gray color. Shows clear cleavage.

Na_2KSb - Has a dull bluish-gray color. Shows clear cleavage.

NaK_2Sb - Has a dull greenish-gray color. Shows clear cleavage.

APPENDIX V

Thermodynamics of Alkali Metal - Antimony Systems

The use of purified argon gas as protective atmosphere and the relatively low vaporization losses of the alkali metals during the tests can be better visualized by thermodynamic means. Potassium has been chosen as an example for this discussion.

Vapor pressure data for potassium metal at several temperatures are listed in the following Table 1.

TABLE 1

Vapor Pressure Data for Potassium Metal (19)

Temperature, °C	Pressure, atm.
227	2.75×10^{-5}
327	8.36×10^{-4}
427	9.37×10^{-3}
527	5.74×10^{-2}
627	2.34×10^{-1}
727	7.37×10^{-1}

No thermodynamic data on any of the alkali metal - antimony systems were available in the literature. As an approximation, data on the potassium - bismuth system, taken from reference (19) and listed in Table 2,

has been used for discussion purposes. This can be considered an accurate approximation since bismuth belongs to the same group of antimony in the periodic table; also, the K-Sb and K-Bi phase diagrams are very similar.

TABLE 2

Thermodynamic Activity and Activity Coefficient of Potassium in the K-Bi System at 575°C (19)

Potassium, Atom Fraction	a_K	γ_K
0.1	4.13×10^{-6}	4.13×10^{-5}
0.2	1.40×10^{-5}	6.98×10^{-5}
0.3	4.68×10^{-5}	1.56×10^{-4}
0.4	2.01×10^{-4}	5.03×10^{-4}
0.5	1.11×10^{-3}	2.22×10^{-3}
0.6	6.82×10^{-3}	1.14×10^{-2}

Assuming the values for a_K in the K-Sb system to be similar to the values of that in the K-Bi system, we can make the following conclusion. The activity coefficient of potassium or any alkali metal in alloys with antimony have a very great negative deviation.

To give an idea of the actual values of the partial pressure of oxygen in equilibrium with the K-K_2O system and the vapor pressure of potassium alloys with antimony, the author has taken the values of a_K in the K-Bi system and used them in calculations for the K-Sb system. The obtained values are listed in Table 3.

The following equations have been used:

$$K = \frac{(a_{K_2O})^2}{(a_K)^4 \times p_{O_2}} = \frac{1}{(a_K)^4 \times p_{O_2}}$$

and $$p_K\text{alloy} = p_K\text{pure} \times a_K\text{alloy}.$$

TABLE 3

Oxygen Partial Pressures in Equilibrium in the System K-K_2O and Potassium Vapor Pressure in Antimony Alloys, at 575°C

Potassium, atom fraction	p_{O_2}, atm.	Potassium Vapor Pressure, atm.
1.0	2.5×10^{-38}	1.5×10^{-1}
0.6	1.1×10^{-29}	1.0×10^{-4}
0.5	2.0×10^{-26}	1.6×10^{-4}
0.4	1.5×10^{-23}	3.0×10^{-5}
0.3	5.3×10^{-21}	7.0×10^{-6}
0.2	6.5×10^{-19}	2.1×10^{-6}
0.1	8.6×10^{-17}	6.2×10^{-7}

These results give an explanation for the successful use of purified argon gas as an effective protective atmosphere, and justify the relatively low vaporization losses during the tests.

LITERATURE CITED

1. Mathewson, C. H.: Natrium-Blei-, Natrium-Kadmium-, Natrium-Wismit- und Natrium-Antimonlegierungen, Z. anorg. Chem., 50, 192-195 (1906).
2. Parravano, N.: Gli Antimoniuri di Potassio, Gazz. chem. ital., 45 485-489 (1915).
3. Sommer, A. H.: New Photoemissive Cathodes of High Sensitivity, Rev. Scient. Instr., 26, 725 (1955).
4. Zintl, E., and Dullenkopf, W.: Polyantimonide, Polywismutide und ihr Übergang in Legieruargen, Z. Phys. Chem., B16, 183 (1932).
5. Gorlich, P.: Z. F. phys., 101, 335 (1936).
6. Sommer, A. H.: Photoelectric Alloys of Alkali Metals, Proc. Phys. Soc., 55, 145 (1943).
7. Jack, K. H., and Wachtel, M. M.: The Characterization and Crystal Structure of Caesium Antimonide, a Photo-electric Surface Material, Proc. roy. Soc., A239, 46-60 (1957).
8. Spicer, W. E.: Photoemissive Photoconductive and Optical Absorption Studies of Alkali-Sb Compounds, Phys. Rev., 112, 114 (1948).

9. Herold, P. G.: Development of the K-Na-Sb Phase Diagram and Photoemission Studies of Compositions in this System. Research proposal submitted to the Colorado School of Mines Foundation, Inc. (1964).

10. Scheer, J. J., and Zalm, P.: Crystal Structure of Sodium-Potassium Antimonide (Na_2KSb), Philips Research Repts., 14, 143 (1959).

11. McCarroll, W. H.: Phases in the Photoelectric Sodium-Potassium-Antimony System, J. Phys. Chem Solids, 16, 30-36 (1960).

12. Hansen, M.: Constitution of Binary Alloys, McGraw-Hill Book Co., Inc., New York (1958).

13. Cromer, D. T.: The Crystal Structure of NaSb, Acta Cryst., 12, 41 (1959).

14. Darken, L., and Burry, R.: Physical Chemistry of Metals, McGraw-Hill Book Co., Inc., New York, 349 (1953).

15. MacDonald, D. K. C., Pearson, W. B., and Towle, L. T.: An Investigation of the Sodium-Potassium Equilibrium Diagram, Can. J. Phys., 34, 389 (1956).

16. van Rossen Hoogendijk van Bleiswijk, G.L.C.M.: Über das Austanddiagramm der Kalium-Natriumlegierungen, Z. anorg. Chem., 74, 152 (1912).

17. Jänecke, E.: Über die Legierungen von Na-K-Hg-Cd, Z. Metallkunde, 20, 115 (1928).

18. Rinck, E.: Diagrammes de Solidification des Alliages Formes par Deux Metaux Alkalins. Alliages Sodium-Potassium, Compt. rend., 197, 49 (1933).

19. Hultgren, R., Orr, R., Anderson, P., and Kelley, K.: Selected Values of Thermodynamic Properties of Metals and Alloys, John Wiley & Sons, Inc., New York (1963).

20. Smith, M. C.: Alloy Series in Physical Metallurgy, Harper & Bros., Publishers, New York (1956).

21. Kubachewski, O., and Evans, E. L.: Metallurgical Thermodynamics, Academic Press, New York (1951).